

Optimal design of acoustic metamaterial cloaks under uncertainty

Peng Chen^a, Michael R. Haberman^b, Omar Ghattas^{a,b,c}

^a*Oden Institute for Computational Engineering & Sciences, The University of Texas at Austin, Austin, TX 78712
(peng@oden.utexas.edu)*

^b*Walker Department of Mechanical Engineering, The University of Texas at Austin, Austin, TX 78712
(haberman@utexas.edu)*

^c*Department of Geological Sciences, The University of Texas at Austin, Austin, TX 78712 (omar@oden.utexas.edu)*

Abstract

In this work, we consider the problem of optimal design of an acoustic cloak under uncertainty and develop scalable approximation and optimization methods to solve this problem. The design variable is taken as an infinite-dimensional spatially-varying field that represents the material property, while an additive infinite-dimensional random field represents the variability of the material property or the manufacturing error. Discretization of this optimal design problem results in high-dimensional design variables and uncertain parameters. To solve this problem, we develop a computational approach based on a Taylor approximation and an approximate Newton method for optimization, which is based on a Hessian derived at the mean of the random field. We show our approach is scalable with respect to the dimension of both the design variables and uncertain parameters, in the sense that the necessary number of acoustic wave propagations is essentially independent of these dimensions, for numerical experiments with up to one million design variables and half a million uncertain parameters. We demonstrate that, using our computational approach, an optimal design of the acoustic cloak that is robust to material uncertainty is achieved in a tractable manner. The optimal design under uncertainty problem is posed and solved for the classical circular obstacle surrounded by a ring-shaped cloaking region, subjected to both a single-direction single-frequency incident wave and multiple-direction multiple-frequency incident waves. Finally, we apply the method to a deterministic large-scale optimal cloaking problem with complex geometry, to demonstrate that the approximate Newton method's Hessian computation is viable for large, complex problems.

Keywords: acoustic cloak, optimal design under uncertainty, PDE-constrained optimization, Taylor approximation, approximate Newton method, scalability, high dimensionality

1. Introduction

Research on acoustic and elastic metamaterials is a product of a unique combination of technological advances that have been made over the last three decades to achieve extraordinary

¹This research was partially funded by the Department of Energy, Office of Science, Office of Advanced Scientific Computing Research, Mathematical Multifaceted Integrated Capability Centers (MMICCS) program under award de-sc0019303; the Simons Foundation under award 560651; the Air Force Office of Scientific Research, Computational Mathematics program under award FA9550-17-1-0190; and the National Science Foundation, Division of Advanced Cyberinfrastructure under award ACI-1550593.

redirection, absorption, or amplification of acoustic or elastic wave disturbances by designing the sub-wavelength structure of the medium through which mechanical disturbances propagate [1, 2, 3]. Of specific interest here is the field of acoustic and elastic metamaterials that make use of the convergence of novel concepts in physics with advances in technology and computational methods, primarily the field of additive manufacturing (AM) [4, 5, 6] and access to robust computational tools [7, 8, 9, 10]. The simultaneous rapid maturation of AM and computational methods allows researchers to rapidly simulate, build, and test elaborate structures for acoustic wave manipulation that follow from rigorous mathematical predictions such as transformation acoustics (TA) [11, 12]. TA is a mathematical approach that uses coordinate transformations to map the physical space to a different space of interest using a one-to-one map between the two domains [11, 13, 14, 12]. The mathematical map is then used to determine the material properties in the region of the transformed fields that produce the same effect in the physical space. For example, mapping the acoustic field in a finite volume surrounding a small scatterer to that of a shell surrounding a larger object allows one to determine the material properties within the shell that produce a cloak capable of rerouting acoustic waves around the large object. This approach provides a forward model for the determination of the material properties required to generate an acoustic cloak using TA.

However, the true research challenge is to define material microstructure that generates effective material properties that meet the prescription provided by TA for the frequencies of interest using existing materials and manufacturing methods. Coordinate transformation and its application to the manipulation of electromagnetic waves preceded the application of coordinate transformations to acoustic waves. Indeed the concept of transformation acoustics was initially facilitated by utilizing the direct analogy that exists in two dimensions between Maxwell's equations and the equations describing acoustic wave propagation [11, 12]. Slight differences in the coordinate transformation were found for 3D geometries, arising from the fundamental differences of 3D wave propagation for transverse (electromagnetic) and longitudinal (acoustic) waves [13]. Although highly anisotropic, such effective fluids could be theoretically realized using alternating layered structures with ordinary (isotropic) fluid-like properties [15] or frequency-dependent waveguide designs [16]. However, coordinate transformation of elastic materials, in which compressional and transverse shear waves co-exist, require a far more exotic metamaterial with a fundamentally new type of microstructure: pentamode (PM) materials. PM materials are defined as materials whose stiffness tensors have only one non-null eigenvalue out of a possible six [14]. In other words, these materials have five deformation modes that can be imposed without storing energy in the material [14] and they can therefore be thought of as quasi-fluids. While the transformation acoustics provides an exact analytical solution for the material properties required to create a perfect cloak, it suffers from several serious drawbacks. The primary problem with this approach is that while it prescribes the material properties required to achieve cloaking, it cannot define the sub-wavelength structure that will generate the required properties. In this sense, coordinate transformation methods are simply analytical methods to solve forward problems and shed no light on how the behavior of interest can be generated. The vast majority of acoustic cloaking research has therefore relied on physical insight and researcher creativity to find material structures that generate the required material properties to achieve cloaking of an object.

A powerful technique to achieve cloaking can be accomplished using a plasmonic cloak, also known as a scattering cancellation (SC) cloak, which is a non-resonant means of eliminating the field scattered from an object, thereby hiding it from detection. This was originally applied and demonstrated for electromagnetic waves [17, 18] using plasmonic materials to achieve the

necessary cloaking layer properties. The SC approach to cloaking was subsequently shown to be an effective means of cloaking acoustic waves [19, 20]. Unlike cloaks developed using a coordinate transformation approach [21, 14], only the scattered field in the surrounding medium is eliminated, and therefore this solution does not limit the incident wave from interacting with the object. As a result, there is no restriction on the use of isotropic materials to create a plasmonic cloak, and it may be used to suppress the scattering from sensors [22, 23, 24]. In previous work, the composition of an SC cloak for cylindrical or spherical objects was found by minimizing the total scattering cross-section of the object and cloak by varying the number, radius, and material properties of layers surrounding the object to be cloaked [17, 19, 20, 25]. This approach was later extended to the design of cloaks for non-spherical objects and collections of objects [26]. Further, the SC method is well-suited for numerical approaches to determining material property distributions required to achieve cloaking. It has been applied to design three-dimensional cloaks with unidirectional performance [27] and two-dimensional cloaks that exploit Bézier scatterers in the cloaking region to minimize the scattered field [28]. A similar computational approach employs a gradient-based optimization algorithm to minimize the total scattering cross section (TCSC) of a collection of rigid or elastic cylinders surrounded cylindrical scatterers that collectively act as a unidirectional cloak [29]. Similar work by Andkjær and Sigmund employed topology optimization to design a cloak that used a small number of scatterers in the cloaking region to conceal a circular region in two-dimensional space from detection via airborne sound [30]. Each of these contributions employ numerical optimization to determine the geometry and properties in the cloaking region. However, these works and many others have only paid cursory attention to the influence that variation in material properties or geometry may have on cloaking performance. Further, to the authors' knowledge, there has been no effort to study how cloaking design may change when variability is accounted for in the design. Given that fabrication of cloaks must consider real-world variation in as-built material properties or achievable levels of manufacturing precision, addressing this problem is central to the creation of reliable acoustics cloaks.

In the optimal design of acoustic cloaks, uncertainties may arise from various sources, including material property variability and flaws or deviations introduced by the manufacturing process. It is therefore important to take uncertainties into account in order to design a robust cloak that can cancel the scattered wave as much as possible under different realizations of the uncertainty. For this purpose we consider the problem of optimal design of an acoustic cloak under uncertainty. While our methodology can be applied more generally, the case considered here is that of time-harmonic acoustic wave propagation and scattering from an impenetrable obstacle. The wave motion in the background medium and the cloak is described by the Helmholtz equation with varying wavenumber, i.e., a spatially-varying sound speed in the cloaking region. We model the sound speed in the cloak as a perturbation of the sound speed in the host homogeneous medium by an exponential factor, which is taken as an infinite-dimensional spatially-varying design variable field. The uncertain parameter is modeled as a Gaussian random field that is additive to the design variable supported in the same cloak region. The objective for the optimal design is to minimize the scattered wave outside the obstacle and cloak region, for which we take a suitable norm of this quantity as the design objective. Since the design objective depends on the uncertain parameter through the Helmholtz equation, it is also an uncertain or random function. To account for this uncertainty in the optimal design, we consider both the mean and the variance of the design objective and minimize an objective functional including a weighted combination of the two. To promote the sparsity of the design material, we add a weighted L^1 -norm of the design variable as a penalty to the objective functional.

The optimal design under uncertainty problem presented above leads to a random partial differential equation (PDE)-constrained optimization problem, which after appropriate discretization results in high-dimensional uncertain parameters and optimization variables. Solution of this class of problems faces enormous challenges, and has received increasing attention in recent years [31, 32, 33, 34, 35, 36, 37, 38, 39, 40, 41, 42, 43, 44, 45, 46, 47, 7, 48, 9, 49]. One prominent challenge is the evaluation of the high-dimensional integral involved in the mean and variance of the design objective. A straightforward approach is to use Monte Carlo integration, which amounts to the sample average approximation (SAA) method, which has a convergence rate ($O(M^{-1/2})$ with M samples) that does not depend on the parameter dimension. Nevertheless, its convergence is often too slow, so a large number of samples is required to achieve a certain required accuracy. Since one PDE has to be solved for each sample, this leads to an optimization constrained by a large number of PDEs, and thus this method is usually computationally prohibitive. As an alternative, rapidly-convergent methods such as stochastic Galerkin and collocation have been applied [33, 34, 37, 35, 36, 39, 38, 40, 42, 45]. However, they often face the curse of dimensionality, i.e., the computational complexity grows exponentially with respect to the uncertain parameter dimension, which prevents their use for problems with high-dimensional uncertain parameters.

Another challenge is that discretization of the design variable field leads to a high-dimensional optimization problem. A simple steepest descent based method will require far too many optimization iterations to converge, while a Newton method may converge rapidly but require the computation of the Hessian of the objective functional acting in given directions, which is often too complex for sophisticated approximations of the objective functional as we employ here. In this work, we propose a computational approach based on a Taylor approximation for the evaluation of the high-dimensional integral in the objective functional and an approximate Newton method for the high-dimensional optimization problem. We employ the Taylor approximation based optimization strategy proposed in [7, 9, 49], by which we approximate the design objective by its (quadratic) Taylor expansion with respect to the uncertain parameter and compute the trace of the preconditioned Hessian resulting from this approximation by a randomized singular value decomposition (SVD) algorithm. The computational complexity measured in terms of the number of PDE solves depends only on the—often small and dimension independent—number of dominant eigenvalues of the preconditioned Hessian, and not on the nominal large uncertain parameter dimension. Thus this approximation is scalable with respect to the parameter dimension. To solve the high-dimensional optimization problem, we propose an approximate Newton method in which the Hessian of the objective functional based on the quadratic Taylor approximation, which is too complex to compute, is approximated by that of the deterministic objective functional, i.e., one that is evaluated at the mean of the random variable. Provided the uncertainty is not too large, e.g., the noise-to-signal ratio or the ratio between the magnitude of the uncertain parameter and that of the design variable is less than 20% in our application, the deterministic Hessian provides a good approximation of the true Hessian, thus leading to an optimization method that is (effectively) scalable with respect to the optimization variable dimension.

We apply the proposed computational approach to the optimal design under uncertainty of the acoustic cloak in several different settings. A classical circular obstacle surrounded by a ring-shaped cloak is used to demonstrate the efficacy of optimal design under uncertainty and our scalable computational approach. First, we consider a deterministic approximation of the objective functional, which results in a deterministic optimal design problem. In this setting, the scattered field is efficiently eliminated by the optimization. Second, we compare this design with the optimal design under uncertainty and show that the latter achieves a significant

reduction in variability of the scattered field relative to the deterministic optimal design. Third, to demonstrate the scalability of the Taylor approximation and the approximate Hessian-based Newton optimization methods, we solve the optimal design problem for a sequence of refined finite element discretizations with dimension up to half a million for the uncertain parameters and one million for the design variables. Scalability with respect to the dimensions of the uncertain parameters and the design variables is demonstrated by dimension-independence of (1) the convergence of the optimizer, (2) the spectral decay of the eigenvalues of the preconditioned Hessian of the design objective with respect to the uncertain parameters, and (3) the accuracy of the Taylor approximation. Fourth, we extend the optimal design problem with single direction, single frequency incident wave to one with multiple directions and multiple frequencies, and demonstrate the efficacy of the acoustic cloak. Finally, we consider a more complex geometry representative of a stealth aircraft, for which we also obtain an effective acoustic cloak.

The rest of the paper is organized as follows: In Section 2, we formulate the optimal design of the acoustic cloak under uncertainty problem, including the governing Helmholtz PDE constraint, the uncertain parameters and design variables, and the formulation of the mean-variance objective functional and sparsifying penalty term. Section 3 presents the approximation methods of the mean-variance functional, including the deterministic approximation, the sample average approximation, and the Taylor approximation with randomized SVD computation of the resulting trace. The optimization method is presented in Section 4, in which the computation of the gradient and (approximate) Hessian of the objective functional with respect to the design variables, as well as the approximate Newton method itself, are derived. Several numerical experiments for the optimal design of an acoustic cloak are presented in Section 5, which is followed by conclusions in Section 6.

2. Problem formulation

In this section, we formulate the problem of optimal design of an acoustic cloak under uncertainty. The forward problem consists of time-harmonic acoustic wave scattering in an inhomogeneous medium described by the Helmholtz equation, in a region truncated by perfectly matched layer. We describe the representation of the design variables and uncertain parameters, the mean-variance objective functional, and the formulation of the optimal design under uncertainty problem.

2.1. Acoustic wave scattering

The time-harmonic acoustic wave scattering of an incident wave in a host medium from an impenetrable obstacle surrounded by an inhomogeneous metamaterial medium is governed by the following Helmholtz equation [50]:

$$\Delta u + k^2 u = (k_0^2 - k^2) u^{\text{inc}} \quad \text{in } \mathbb{R}^d \setminus D_o, \quad (1a)$$

$$\nabla u \cdot n = -\nabla u^{\text{inc}} \cdot n \quad \text{on } \partial D_o, \quad (1b)$$

$$\lim_{r \rightarrow \infty} r^{(d-1)/2} \left(\frac{\partial u}{\partial r} - iku \right) = 0, \quad (1c)$$

where \mathbb{R}^d is the physical space of dimension $d = 2, 3$, $D_o \subset \mathbb{R}^d$ is the region of the obstacle with boundary ∂D_o . u^{inc} is the incident wave given by $u^{\text{inc}} = e^{ik_0 x \cdot b}$ in direction $b \in \mathbb{R}^d$ with the complex unit $i = \sqrt{-1}$; u is the scattered wave; the total wave is given by $u^t = u + u^{\text{inc}}$. In addition,

k_0 is the wavenumber in the background medium given by the positive constant $k_0 = \omega/c_0$ with frequency ω and constant speed of sound c_0 in the host medium, while $k(x) = \omega/c(x)$ is a spatially-varying wavenumber in the inhomogeneous medium. $c(x)$ denotes the speed of sound at $x \in \mathbb{R}^d$ in the inhomogeneous medium. A *sound-hard* boundary condition is imposed on the boundary ∂D_o in (1b) for the impenetrable obstacle, where n denotes the outward unit normal vector along ∂D_o . Eq. (1c) is the *Sommerfeld radiation condition* that guarantees that the scattered wave is outgoing, which is realized by a *perfectly matched layer* (PML) condition [51]. $r(x) = |x|$ denotes the distance from x to the origin.

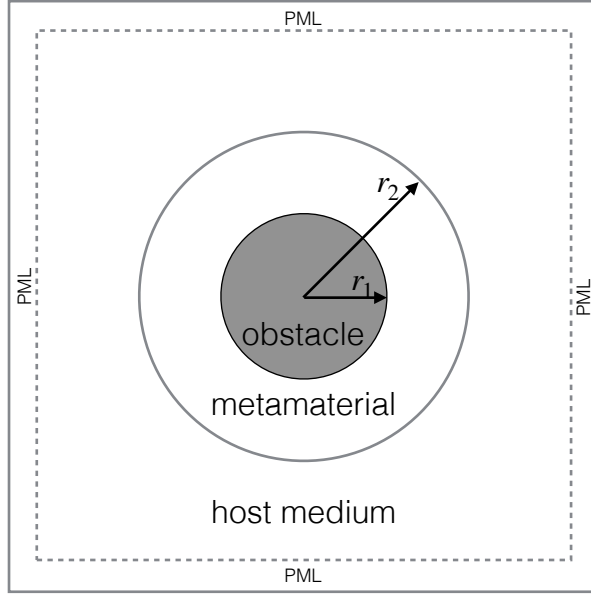


Figure 1: Sketch of the domain for acoustic wave scattering in an inhomogeneous medium.

2.2. Weak formulation with PML condition

To solve the problem numerically, we consider a bounded and square computational domain $D \subset \mathbb{R}^d \setminus D_o$ that includes the inhomogeneous metamaterial medium as shown in Fig. 1, and use a PML condition [51] on its outgoing boundary to prevent reflection of the scattered wave as imposed by (1c). In two dimensions, i.e., $d = 2$, the PML condition leads to [51]

$$\partial_{x_1} \left(\frac{s_{x_2}}{s_{x_1}} \partial_{x_1} u \right) + \partial_{x_2} \left(\frac{s_{x_1}}{s_{x_2}} \partial_{x_2} u \right) + k^2 s_{x_1} s_{x_2} u = (k_0^2 - k^2) u^{\text{inc}} \quad \text{in } D, \quad (2)$$

where

$$s_{x_1} = 1 + \frac{\sigma_{x_1}}{ik}, \quad s_{x_2} = 1 + \frac{\sigma_{x_2}}{ik}, \quad (3)$$

where $k(x) = k_0 \sqrt{n(x)} = \omega/c(x)$, σ_{x_1} and σ_{x_2} are real valued continuous functions in the PML region D_p , which depend only on the physical coordinate x_1 and x_2 , respectively. Outside the PML region, i.e., $D \setminus D_p$, we have $\sigma_{x_1} = 0$ and $\sigma_{x_2} = 0$, so that (2) becomes the same equation as

(1a). The wave function u is complex valued, which can be written as $u = u_1 + iu_2$ with the real and imaginary parts u_1 and u_2 , respectively. Then (2) can be written as a set of two equations in D with real coefficients as

$$\begin{aligned} \partial_{x_1}(a_1\partial_{x_1}u_1 - a_2\partial_{x_1}u_2) + \partial_{x_2}(a_3\partial_{x_2}u_1 - a_4\partial_{x_2}u_2) + b_1u_1 - b_2u_2 &= (k_0^2 - k^2)u_1^{\text{inc}} \\ \partial_{x_1}(a_1\partial_{x_1}u_2 + a_2\partial_{x_1}u_1) + \partial_{x_2}(a_3\partial_{x_2}u_2 + a_4\partial_{x_2}u_1) + b_1u_2 + b_2u_1 &= (k_0^2 - k^2)u_2^{\text{inc}} \end{aligned} \quad (4)$$

where $u_1^{\text{inc}} = \cos(k_0x \cdot b)$, $u_2^{\text{inc}} = \sin(k_0x \cdot b)$; the coefficients are given by

$$a_1 = \frac{k^2 + \sigma_{x_1}\sigma_{x_2}}{k^2 + \sigma_{x_1}^2}, \quad a_2 = \frac{k(\sigma_{x_1} - \sigma_{x_2})}{k^2 + \sigma_{x_1}^2}, \quad a_3 = \frac{k^2 + \sigma_{x_1}\sigma_{x_2}}{k^2 + \sigma_{x_2}^2}, \quad a_4 = \frac{k(\sigma_{x_2} - \sigma_{x_1})}{k^2 + \sigma_{x_2}^2}, \quad (5)$$

and

$$b_1 = k^2 - \sigma_{x_1}\sigma_{x_2}, \quad b_2 = -k(\sigma_{x_1} + \sigma_{x_2}). \quad (6)$$

To state the weak formulation of the equations (4), we introduce the following notation. Let $L^2(D)$ denote the Hilbert space of square-integrable functions in D , and let $H^1(D) := \{v \in L^2(D), |\nabla v| \in L^2(D)\}$, $V = H^1(D) \times H^1(D)$. Then the weak formulation of (4) can be written as: find $u = (u_1, u_2) \in V$, such that

$$A(u, v) = F(v), \quad \forall v = (v_1, v_2) \in V, \quad (7)$$

where the bilinear form $A : V \times V \rightarrow \mathbb{R}$ is given by

$$\begin{aligned} A(w, v) &= \int_D (a_1\partial_{x_1}w_1 - a_2\partial_{x_1}w_2)\partial_{x_1}v_1 + (a_3\partial_{x_2}w_1 - a_4\partial_{x_2}w_2)\partial_{x_2}v_1 \, dx \\ &\quad + \int_D (a_1\partial_{x_1}w_2 + a_2\partial_{x_1}w_1)\partial_{x_1}v_2 + (a_3\partial_{x_2}w_2 + a_4\partial_{x_2}w_1)\partial_{x_2}v_2 \, dx \\ &\quad - \int_D (b_1w_1 - b_2w_2)v_1 + (b_1w_2 + b_2w_1)v_2 \, dx \end{aligned} \quad (8)$$

and the linear form $F : V \rightarrow \mathbb{R}$ is given by

$$F(v) = \int_D (k_0^2 - k^2)u_1^{\text{inc}}v_1 + (k_0^2 - k^2)u_2^{\text{inc}}v_2 \, dx - \int_{\partial D_o} \nabla u_1^{\text{inc}} \cdot nv_1 + \nabla u_2^{\text{inc}} \cdot nv_2 \, ds. \quad (9)$$

2.3. Uncertain parameter and design variable

To manufacture the acoustic cloak, additive manufacturing (AM) offers significant promise since it allows the fabrication of complex parts that cannot be readily created using traditional techniques [52, 5]. Of specific interest here is the potential to construct materials with spatially graded material properties by adjusting process control variables within the build volume. However, this capability is not perfect and errors can be introduced at each manufacturing step. Further, each fabrication approach has some level of uncertainty in the as-built material properties, whose contribution to the final manufacturing accuracy is unclear [53, 54]. In this work, we consider an aggregated uncertainty and incorporate it in the sound speed in the cloak, which is represented by

$$c(x, \omega) = c_0 e^{\zeta(x, \varpi) - \tau(x)}, \quad \forall x \in D_m, \text{ a.e. } \varpi \in \Omega \quad (10)$$

Here, τ is the spatially-varying deterministic design variable field of the cloak in the design region D_m , which exists in a separable Banach space Z . At every $x \in D_m$, $\zeta(x, \cdot)$ is a real valued

random variable defined in the probability space (Ω, \mathcal{F}, P) , with the sample space Ω , a set of events \mathcal{F} , and the probability function $P : \mathcal{F} \rightarrow [0, 1]$. To accommodate the spatial correlation of the random variables $\zeta(x, \cdot)$ at different $x \in D_m$, we consider one of the most popular random fields—*Gaussian random fields* with probability measure $\mu = \mathcal{N}(\bar{\zeta}, C)$ defined in a Hilbert space X with dual X' , where $\bar{\zeta} \in X$ is the mean and C is the covariance operator that can be viewed as an integral operator with suitable covariance kernel. A very general covariance kernel widely used in spatial statistics, geostatistics, machine learning, etc., is the Matérn covariance, which leads to the Gaussian field ζ as a solution of the stochastic fractional PDE [55] with homogeneous Neumann boundary condition

$$\begin{aligned} (-\gamma\Delta + \delta I)^{\alpha/2}(\zeta - \bar{\zeta}) &= W \quad \text{in } D_m, \\ \nabla\zeta \cdot n &= 0 \quad \text{on } \partial D_m, \end{aligned} \quad (11)$$

where W represents the spatial Gaussian white noise with unit variance, I , ∇ , and Δ are the identity, gradient, and Laplace operators, and n is the outward unit normal vector along ∂D_m . Thus $C = (-\gamma\Delta + \delta I)^{-\alpha}$, with $\alpha > d/2$ controlling the *regularity*, δ and γ controlling the *variance*, and γ/δ controlling the *correlation length* of ζ . Moreover, C is self-adjoint, positive, and of trace class. Therefore, sampling ζ involves solution of the elliptic stochastic PDE (11). Generalizations of the stochastic PDE (11) may be used to model non-stationary, non-isotropic, complex random fields [55].

2.4. Optimal design of acoustic cloak

Recall that D_o and D_m denote the regions of the obstacle and the metamaterial cloak surrounding the obstacle, respectively; let $D_h = D \setminus (D_o \cup D_m)$ denote the host medium where we can observe the scattered wave. Our goal is to minimize the scattered wave in D_h so that the obstacle becomes “invisible”, i.e., no wave scattering observed outside of the obstacle and its cloak. To achieve this, we define the design objective as

$$Q(u) = \int_{D_h} (|u_1|^2 + |u_2|^2) dx, \quad (12)$$

which is the scattered wave amplitude measured in the L^2 -norm. The design objective Q is random and depends on the random (field) variable ζ through the random scattered wave u as a solution of (7), where we write $u = u(\zeta, \tau)$ to indicate that the scattered wave depends on the random variable ζ and the design variable τ . To quantify the randomness of Q , we use a mean-variance measure and consider the following objective functional to be minimized

$$J(\tau) = \mathbb{E}[Q](\tau) + \beta_V \text{Var}[Q](\tau) + \beta_P P(\tau), \quad (13)$$

where the mean and variance of Q are given by

$$\mathbb{E}[Q](\tau) = \int_X Q(u(\zeta, \tau)) d\mu \quad \text{and} \quad \text{Var}[Q](\tau) = \int_X (Q(u(\zeta, \tau)) - \mathbb{E}[Q](\tau))^2 d\mu, \quad (14)$$

where the integration is taken with respect to the Gaussian measure $\mu = \mathcal{N}(\bar{\zeta}, C)$ in X . $P(\tau)$ is a penalty term on the deterministic control $\tau \in Z$. To promote the sparsity of the material in the cloak, we consider an L^1 -norm for τ , i.e.,

$$P(\tau) = \int_{D_m} |\tau(x)| dx \approx \int_{D_m} (\tau^2(x) + \varepsilon)^{1/2} dx, \quad (15)$$

where we use the approximate form with a small $\varepsilon > 0$ to make $P(\tau)$ differentiable with respect to τ and thus facilitate gradient based optimization. Further, $\beta_V > 0$ and $\beta_P > 0$ in (13) are scalar parameters that weight the importance of the variance and penalty with respect to the mean. The problem of the optimal design of the acoustic cloak under uncertainty is finally formulated as the PDE-constrained stochastic optimization problem

$$\min_{\tau \in Z} J(\tau), \quad \text{subject to (7)}. \quad (16)$$

2.5. Optimal design with multiple directions and frequencies

In the above formulation of the optimal design of the acoustic cloak under uncertainty, we consider only one direction b and one frequency ω for the incident wave $u^{\text{inc}} = e^{ik_0 x \cdot b}$ where $k_0 = \omega/c_0$. In this section, we extend the formulation to incident waves with multiple directions and multiple frequencies. For notational clarity, for direction b_i and/or frequency ω_i , $i = 1, \dots, I$ for $I \in \mathbb{N}$, we write the weak formulation (7) as: find $u^i = (u_1^i, u_2^i) \in V$ such that

$$A_i(u^i, v^i) = F_i(v^i), \quad \forall v^i = (v_1^i, v_2^i) \in V, \quad (17)$$

and write the design objective (12) as

$$Q_i = Q(u^i) = \int_{D_n} (|u_1^i|^2 + |u_2^i|^2) dx. \quad (18)$$

The objective functional (13) then becomes

$$\mathcal{J}(\tau) = \sum_{i=1}^I (\mathbb{E}[Q_i](\tau) + \beta_V \text{Var}[Q_i](\tau)) + \beta_P P(\tau), \quad (19)$$

where the mean, variance, and penalty are given as in (14) and (15). Therefore, the optimal design problem with multiple directions and frequencies becomes

$$\min_{\tau \in Z} \mathcal{J}(\tau), \quad \text{subject to (17)}, \quad i = 1, \dots, I. \quad (20)$$

Note that the approximation and optimization methods developed in the rest of the paper for the optimal design problem (16) with single direction and frequency can be straightforwardly extended to the optimal design problem (20) with multiple directions and frequencies. For simplicity, we present methods for only the former case.

3. Approximation of the mean-variance objective

In this section, we present three classes of approximation methods for the evaluation of the mean and variance in the objective functional: one is a deterministic approximation with the design objective evaluated only at the mean of the random variable ζ , the second is a classical sample average approximation, and the third is a quadratic Taylor approximation. For notational simplicity, whenever there is no ambiguity, we denote $Q(\zeta)$ for the random objective $Q(u(\zeta, \tau))$ at design $\tau \in Z$, and keep in mind that the dependence of Q on ζ is implicit through u .

3.1. Deterministic approximation

In this approach, we evaluate the design objective at only one fixed sample, e.g., the mean $\bar{\zeta}$ of the random variable ζ , so that the expectation and variance of the design objective are approximated as

$$\mathbb{E}[Q] \approx Q(\bar{\zeta}) \text{ and } \text{Var}[Q] \approx 0, \quad (21)$$

which leads to a deterministic optimization problem at $\bar{\zeta}$.

3.2. Sample average approximation

Let ζ_m , $m = 1, \dots, M$, denote i.i.d. random samples drawn from the Gaussian distribution $\mathcal{N}(\bar{\zeta}, C)$, then the mean of Q can be approximated by the average

$$\mathbb{E}[Q] \approx \frac{1}{M} \sum_{m=1}^M Q(\zeta_m), \quad (22)$$

which is known as *sample average approximation* or *Monte Carlo approximation*. The variance can be approximated similarly by the average

$$\text{Var}[Q] = \mathbb{E}[Q^2] - (\mathbb{E}[Q])^2 \approx \frac{1}{M} \sum_{m=1}^M Q^2(\zeta_m) - \left(\frac{1}{M} \sum_{m=1}^M Q(\zeta_m) \right)^2. \quad (23)$$

We remark that to balance the approximation errors of the mean and variance, different numbers of i.i.d. random samples can be used for the mean and variance evaluation.

3.3. Taylor approximation

Following the previous work [7, 9], we present a Taylor approximation for the design objective Q and the closed form of the mean and variance based on the Taylor approximation. A formal functional Taylor approximation of the objective Q at the mean $\bar{\zeta}$, truncated with K terms, is written as

$$T_K Q(\zeta) = \sum_{k=0}^K \partial_{\zeta}^k Q(\bar{\zeta})(\zeta - \bar{\zeta})^k, \quad (24)$$

where we assume that Q is K -th order Fréchet differentiable with respect to ζ . The term $\partial_{\zeta}^k Q(\bar{\zeta})(\zeta - \bar{\zeta})^k$ denotes the k -th order (tensor) derivative $\partial_{\zeta}^k Q(\bar{\zeta})$ at $\bar{\zeta}$ acting on $\zeta - \bar{\zeta}$ in each of the k directions, $k = 1, \dots, K$. For $K = 2$, we can write the Taylor approximation (24) more explicitly as

$$T_2 Q(\zeta) = \bar{Q} + \langle \bar{g}, \zeta - \bar{\zeta} \rangle + \frac{1}{2} \langle \bar{\mathcal{H}}(\zeta - \bar{\zeta}), \zeta - \bar{\zeta} \rangle, \quad (25)$$

where $\bar{Q} \in \mathbb{R}$, $\bar{g} \in X'$, and $\bar{\mathcal{H}} : X \rightarrow X'$ denote the objective and its gradient and Hessian with respect to ζ , evaluated at the mean $\bar{\zeta}$, respectively, and $\langle \cdot, \cdot \rangle = {}_{X'} \langle \cdot, \cdot \rangle_X$ represents the duality pairing in $X' \times X$. Since ζ is a Gaussian field, the mean and variance of the Taylor approximation of the objective truncated at the quadratic term can be written explicitly as [7]

$$\mathbb{E}[T_2 Q] = \bar{Q} + \frac{1}{2} \text{tr}(C\bar{\mathcal{H}}) \quad \text{and} \quad \text{Var}[T_2 Q] = \langle \bar{g}, C\bar{g} \rangle + \frac{1}{2} \text{tr}((C\bar{\mathcal{H}})^2), \quad (26)$$

where we recall that $C : X' \rightarrow X$ is the covariance of ζ , and $\text{tr}(\cdot)$ denotes the trace, with

$$\text{tr}(C\bar{\mathcal{H}}) = \sum_{n \geq 1} \lambda_n \text{ and } \text{tr}((C\bar{\mathcal{H}})^2) = \sum_{n \geq 1} \lambda_n^2. \quad (27)$$

Here, $(\lambda_n)_{n \geq 1}$ are the eigenvalues of $C\bar{\mathcal{H}}$, which are equivalent to the generalized eigenvalues of $(\bar{\mathcal{H}}, C^{-1})$, i.e., in weak form we can write

$$\langle \bar{\mathcal{H}}\psi_n, \phi \rangle = \langle \lambda_n C^{-1}\psi_n, \phi \rangle \quad \forall \phi \in X, \quad n \geq 1, \quad (28)$$

where $(\psi_n)_{n \geq 1} \in X$ are the generalized eigenfunctions that satisfy the C^{-1} -orthonormality condition

$$\langle C^{-1}\psi_n, \psi_m \rangle = \delta_{mn}, \quad m \geq 1, n \geq 1. \quad (29)$$

3.3.1. Randomized algorithm

It is intractable to solve the generalized eigenvalue problem (28) for all of the eigenvalues. In practice, these (absolute) eigenvalues decay rapidly as proven for the Hessians of some model problems and numerically demonstrated for many others [10, 56, 57, 58, 59, 60, 61, 62, 7, 63, 64, 65, 66, 67, 68, 69, 9, 70, 71, 72]. Therefore, we can compute the dominant eigenvalues $\lambda_1, \dots, \lambda_N$, with $|\lambda_1| \geq \dots \geq |\lambda_N| \geq \lambda_n$ for any $n > N$, and approximate the trace by

$$\text{tr}(C\bar{\mathcal{H}}) \approx \sum_{n \geq 1}^N \lambda_n \text{ and } \text{tr}((C\bar{\mathcal{H}})^2) \approx \sum_{n \geq 1}^N \lambda_n^2. \quad (30)$$

To solve the generalized eigenvalue problem (28) for the N dominant eigenvalues, we apply a randomized algorithm [73, 74] in Algorithm 1, where H, C^{-1} of dimension $N_h \times N_h$ denote the discrete approximation of $\bar{\mathcal{H}}$ and C^{-1} , e.g., by finite elements. Here, N_h is the number of mesh degrees of freedom representing the discretized field ζ .

Algorithm 1 Randomized algorithm for the generalized eigenvalue problem (H, C^{-1})

Input: the number of eigenpairs N , an oversampling factor $p \leq 10$.

Output: (Λ_N, Ψ_N) with $\Lambda_N = \text{diag}(\lambda_1, \dots, \lambda_N)$ and $\Psi_N = (\psi_1, \dots, \psi_N)$.

1. Draw a Gaussian random matrix $\Omega \in \mathbb{R}^{N_h \times (N+p)}$.
 2. Compute $Y = C(H\Omega)$.
 3. Compute QR factorization $Y = QR$ such that $Q^T C^{-1} Q = I_{N+p}$.
 4. Form $T = Q^T H Q$ and compute eigendecomposition $T = S \Lambda S^T$.
 5. Extract $\Lambda_N = \Lambda(1 : N, 1 : N)$ and $\Psi_N = Q S_L$ with $S_N = S(:, 1 : N)$.
-

We remark that the computational cost of Algorithm 1 is dominated by the Hessian actions $H\Omega$ and HQ , as presented in the next section. These entail $2(N+p)$ forward and adjoint solutions of the Helmholtz equation. The remaining linear algebra in Algorithm 1 is negligible in comparison. The advantages of Algorithm 1 are [9, 70]: (i) the error in the eigenvalues λ_n , $n = 1, \dots, N$, is bounded by the remaining ones λ_n , $n > N$, which is small if they decay rapidly; (ii) the computational cost is dominated by $2(N+p)$ Hessian actions (the application of C on a vector is inexpensive, e.g., it takes only $O(N_h)$ operations by a multigrid solver for C discretized from an elliptic differential operator); (iii) it is scalable as the number of dominant eigenvalues N typically does not depend on the mesh size N_h ; (iv) computing the Hessian actions $H\Omega$ and HQ can be asynchronously parallelized.

3.3.2. ζ -gradient and ζ -Hessian

The Taylor approximation along with the randomized eigensolver require the computation of the gradient of $Q(\zeta)$ with respect to the random parameter field (the “ ζ -gradient”) and the action of the Hessian of $Q(\zeta)$ (the “ ζ -Hessian”) in an arbitrary direction, both evaluated at the mean $\bar{\zeta}$. To do this, we employ a Lagrangian method as in [9, 70]. We begin by forming the Lagrangian

$$L(u, v; \zeta, \tau) = Q(u) + A(u, v; \zeta, \tau) - F(v; \zeta, \tau), \quad (31)$$

where the bilinear form A and the linear form F defined in (8) and (9) depend on the random parameter and design variable ζ, τ through the representation (10). The adjoint variable v is a Lagrange multiplier for the forward Helmholtz equation (7). Then the state u is obtained by setting the variation of the Lagrangian (31) with respect to the adjoint v to zero to obtain the Helmholtz equation evaluated at $\bar{\zeta}$, i.e., find $u \in V$ such that

$$A(u, \tilde{v}; \bar{\zeta}, \tau) = F(\tilde{v}; \bar{\zeta}, \tau) \quad \forall \tilde{v} \in V, \quad (32)$$

which is the same as (7) evaluated at $\bar{\zeta}$. The adjoint variable v is obtained by setting the variation of (31) with respect to the state u to zero to obtain the adjoint Helmholtz equation evaluated at $\bar{\zeta}$, i.e., find $v \in V$ such that

$$A(\tilde{u}, v; \bar{\zeta}, \tau) = -\langle \partial_u Q(u), \tilde{u} \rangle \quad \forall \tilde{u} \in V. \quad (33)$$

Then the gradient of the design objective Q with respect to the random variable ζ evaluated at $\bar{\zeta}$, acting in any direction $\tilde{\zeta} \in X$, is given by the variation of the Lagrangian with respect to ζ , i.e.,

$$\langle \bar{g}, \tilde{\zeta} \rangle = \langle \partial_\zeta L(u, v; \bar{\zeta}, \tau), \tilde{\zeta} \rangle = \langle \partial_\zeta A(u, v; \bar{\zeta}, \tau) - \partial_\zeta F(v; \bar{\zeta}, \tau), \tilde{\zeta} \rangle. \quad (34)$$

Therefore, the computation of ζ -gradient involves the solution of the Helmholtz equation (32) for u and the Helmholtz equation (33) for v .

To compute the Hessian of Q at $\bar{\zeta}$ acting in a given direction $\hat{\zeta} \in X$, we form the second Lagrangian L^H by adding the (weak formulation of the) forward and adjoint Helmholtz equations to the (directional) gradient to obtain

$$\begin{aligned} L^H(u, v, \hat{u}, \hat{v}; \zeta, \hat{\zeta}, \tau) &= A(u, \hat{v}; \zeta, \tau) - F(\hat{v}; \zeta, \tau) \\ &\quad + A(\hat{u}, v; \zeta, \tau) + \langle \partial_u Q(u), \hat{u} \rangle \\ &\quad + \langle \partial_\zeta A(u, v; \zeta, \tau) - \partial_\zeta F(v; \zeta, \tau), \hat{\zeta} \rangle, \end{aligned} \quad (35)$$

where $\hat{v}, \hat{u}, \hat{\zeta}$ are the Lagrange multipliers for the forward Helmholtz equation (32), the adjoint Helmholtz equation (33), and the gradient (34). Proceeding as with the gradient derivation, we set the variation of L^H with respect to v and u to obtain the incremental state variable \hat{u} as the solution of the “incremental forward Helmholtz equation” (evaluated at $\bar{\zeta}$)

$$A(\hat{u}, \tilde{v}; \bar{\zeta}, \tau) = -\langle \partial_\zeta A(u, v; \bar{\zeta}, \tau) - \partial_\zeta F(v; \bar{\zeta}, \tau), \hat{\zeta} \rangle \quad \forall \tilde{v} \in V, \quad (36)$$

and the incremental adjoint variable \hat{v} as the solution of the “incremental adjoint Helmholtz equation” (evaluated at $\bar{\zeta}$)

$$A(\tilde{u}, \hat{v}; \bar{\zeta}, \tau) = -\langle \partial_{uu} Q(u) \hat{u}, \tilde{u} \rangle - \langle \partial_\zeta A(\tilde{u}, v; \bar{\zeta}, \tau), \hat{\zeta} \rangle \quad \forall \tilde{u} \in V. \quad (37)$$

Finally, the Hessian action at $\bar{\zeta}$ in direction $\hat{\zeta}$, tested again $\tilde{\zeta}$, can be evaluated as

$$\begin{aligned} \langle \tilde{H}\hat{\zeta}, \tilde{\zeta} \rangle &= \langle \partial_{\zeta} L^H, \tilde{\zeta} \rangle = \langle \partial_{\zeta} A(u, \hat{v}; \bar{\zeta}, \tau) - \partial_{\zeta} F(\hat{v}; \bar{\zeta}, \tau), \tilde{\zeta} \rangle \\ &\quad + \langle \partial_{\zeta} A(\hat{u}, v; \bar{\zeta}, \tau), \tilde{\zeta} \rangle \\ &\quad + \langle \partial_{\zeta\zeta} A(u, v; \bar{\zeta}, \tau) \hat{\zeta} - \partial_{\zeta\zeta} F(v; \bar{\zeta}, \tau) \hat{\zeta}, \tilde{\zeta} \rangle. \end{aligned} \quad (38)$$

Therefore, each Hessian action involves the solution of the incremental forward Helmholtz equation (36) and the incremental adjoint Helmholtz equation (37). To compute the objective functional (13) with the quadratic Taylor approximation (25) and the randomized algorithm for trace estimation (Algorithm 1), we need to solve one forward Helmholtz equation (32), one adjoint Helmholtz equation (33), and $2(N+p)$ pairs of incremental forward and adjoint Helmholtz equations (36) and (37).

4. Optimization

In the PDE-constrained optimization problem (16), the design variable field is a function over the cloaking region, and is thus high-dimensional after discretization by finite elements. To solve the resulting high-dimensional optimization problem, we propose an approximate Newton method with backtracking line search for globalization, where the Hessian of the objective functional with respect to the design variable, denoted as the τ -Hessian, is approximated by the Hessian evaluated at the mean of the random field, while the gradient, denoted as the τ -gradient, is computed accurately. The Newton system is solved inexactly in matrix-free fashion by a preconditioned conjugate gradient method. In this section, we present the computation of the τ -Hessian at the mean as well as the τ -gradient of the objective functional (13) for both the sample average approximation of Section 3.2 and the Taylor approximation of Section 3.3.

4.1. τ -gradient and τ -Hessian for the deterministic approximation

Using the deterministic approximation of Section 3.1, we obtain the deterministic optimization problem:

$$\begin{aligned} \min_{\tau \in \mathcal{Z}} J_{\bar{\zeta}}(\tau) \quad &\text{where } J_{\bar{\zeta}}(\tau) = Q(u) + \beta_P P(\tau), \\ \text{subject to } &A(u, v; \bar{\zeta}, \tau) = F(v; \bar{\zeta}, \tau) \quad \forall v \in V. \end{aligned} \quad (39)$$

To compute the gradient and Hessian of the objective functional with respect to the design variable τ , we use a Lagrangian method akin to that presented in Section 3.3.2 for the gradient and Hessian of the design objective with respect to the random variable. Specifically, we first form the Lagrangian

$$L_{\bar{\zeta}}(u, v; \bar{\zeta}, \tau) = Q(u) + \beta_P P(\tau) + A(u, v; \bar{\zeta}, \tau) - F(v; \bar{\zeta}, \tau). \quad (40)$$

The state variable u and the adjoint variable v are obtained by setting the variation of this Lagrangian with respect to the adjoint v and the state u to zero and solving the forward and adjoint Helmholtz equations, which leads to the same problems as in (32) and (33). The τ -gradient (the Fréchet derivative of the objective in a direction $\tilde{\tau}$) is then given by

$$\begin{aligned} \langle \nabla_{\tau} J_{\bar{\zeta}}(\tau), \tilde{\tau} \rangle &= \langle \partial_{\tau} L_{\bar{\zeta}}(u, v; \bar{\zeta}, \tau), \tilde{\tau} \rangle \\ &= \langle \beta_P \nabla_{\tau} P(\tau) + \partial_{\tau} A(u, v; \bar{\zeta}, \tau) - \partial_{\tau} F(v; \bar{\zeta}, \tau), \tilde{\tau} \rangle. \end{aligned} \quad (41)$$

To compute the τ -Hessian acting in a direction $\hat{\tau} \in Z$, we form the second Lagrangian

$$\begin{aligned} L_{\bar{\zeta}}^H(u, v, \hat{u}, \hat{v}; \bar{\zeta}, \tau, \hat{\tau}) &= A(u, \hat{v}; \bar{\zeta}, \tau) - F(\hat{v}; \bar{\zeta}, \tau) \\ &\quad + A(\hat{u}, v; \bar{\zeta}, \tau) + \langle \partial_u Q(u), \hat{u} \rangle \\ &\quad + \langle \beta_P \nabla_{\tau} P(\tau) + \partial_{\tau} A(u, v; \bar{\zeta}, \tau) - \partial_{\tau} F(v; \bar{\zeta}, \tau), \hat{\tau} \rangle, \end{aligned} \quad (42)$$

where $\hat{v}, \hat{u}, \hat{\tau}$ are the Lagrange multipliers for the forward Helmholtz equation (32), the adjoint Helmholtz equation (33), and the gradient (41), respectively. Once again, by setting the variation of $L_{\bar{\zeta}}^H$ with respect to v and u to zero, we obtain the incremental state variable \hat{u} as the solution of the incremental forward Helmholtz equation

$$A(\hat{u}, \hat{v}; \bar{\zeta}, \tau) = -\langle \partial_{\tau} A(u, \hat{v}; \bar{\zeta}, \tau) - \partial_{\tau} F(\hat{v}; \bar{\zeta}, \tau), \hat{\tau} \rangle \quad \forall \hat{v} \in V, \quad (43)$$

and the incremental adjoint variable \hat{v} as the solution of the incremental adjoint Helmholtz equation

$$A(\hat{u}, \hat{v}; \bar{\zeta}, \tau) = -\langle \partial_{uu} Q(u) \hat{u}, \hat{u} \rangle - \langle \partial_{\tau} A(\hat{u}, v; \bar{\zeta}, \tau), \hat{\tau} \rangle \quad \forall \hat{u} \in V. \quad (44)$$

Then the τ -Hessian action at τ in a direction $\hat{\tau}$, tested against $\tilde{\tau}$, can be evaluated as

$$\begin{aligned} \langle \nabla_{\tau\tau} J_{\bar{\zeta}} \hat{\tau}, \tilde{\tau} \rangle &= \langle \partial_{\tau\tau} L_{\bar{\zeta}}^H, \tilde{\tau} \rangle \\ &= \langle \partial_{\tau} A(u, \hat{v}; \bar{\zeta}, \tau) - \partial_{\tau} F(\hat{v}; \bar{\zeta}, \tau), \tilde{\tau} \rangle \\ &\quad + \langle \partial_{\tau} A(\hat{u}, v; \bar{\zeta}, \tau), \tilde{\tau} \rangle \\ &\quad + \langle \beta_P \nabla_{\tau\tau} P(\tau) \hat{\tau} + \partial_{\tau\tau} A(u, v; \bar{\zeta}, \tau) \hat{\tau} - \partial_{\tau\tau} F(v; \bar{\zeta}, \tau) \hat{\tau}, \tilde{\tau} \rangle. \end{aligned} \quad (45)$$

Therefore, at each τ , after solving the forward Helmholtz equation (32) and the adjoint Helmholtz equation (33), to compute the τ -Hessian action in each direction $\hat{\tau}$, we need to solve two PDEs—one incremental forward Helmholtz equation (43) and one incremental adjoint Helmholtz equation (44). In Section 4.4, we derive how this capability for computing the action of the τ -Hessian in an arbitrary direction can be used to solve the (approximate) Newton system by conjugate gradients.

4.2. τ -gradient for the sample average approximation

With the sample average approximation (SAA), the optimization problem (16) becomes

$$\begin{aligned} \min_{\tau \in Z} J_{\text{SAA}}(\tau) \\ \text{subject to } A(u_m, v; \zeta_m, \tau) = F(v; \zeta_m, \tau) \quad \forall v \in V, \quad m = 1, \dots, M, \end{aligned} \quad (46)$$

where $u_m = u(\zeta_m, \tau)$ represents the solution at ζ_m and τ , and the SAA of the objective functional, $J_{\text{SAA}}(\tau)$, is given by

$$J_{\text{SAA}}(\tau) = \frac{1}{M} \sum_{m=1}^M Q(u_m) + \frac{\beta_V}{M} \sum_{m=1}^M Q^2(u_m) - \beta_V \left(\frac{1}{M} \sum_{m=1}^M Q(u_m) \right)^2 + \beta_P P(\tau). \quad (47)$$

To compute the τ -gradient of J_{SAA} , we form the Lagrangian

$$\begin{aligned} L_{\text{SAA}}((u_m)_{m=1}^M, (v_m)_{m=1}^M; (\zeta_m)_{m=1}^M, \tau) \\ = J_{\text{SAA}}(\tau) + \sum_{m=1}^M A(u_m, v_m; \zeta_m, \tau) - F(v_m; \zeta_m, \tau), \end{aligned} \quad (48)$$

where $v_m, m = 1, \dots, M$, are the adjoint variables or the Lagrange multipliers. By setting the variation of the Lagrangian with respect to the state u_m to zero for each $m = 1, \dots, M$, we obtain: find $v_m \in V$ such that

$$A(\tilde{u}, v_m; \zeta_m, \tau) = C_m \langle \partial_u Q(u_m), \tilde{u} \rangle \quad \forall \tilde{u} \in V, \quad m = 1, \dots, M, \quad (49)$$

where the constant C_m is given by

$$C_m = -\frac{1}{M} \left(1 + 2\beta_V Q(u_m) - 2\beta_V \left(\frac{1}{M} \sum_{m=1}^M Q(u_m) \right) \right), \quad m = 1, \dots, M. \quad (50)$$

The τ -gradient of $J_{\text{SAA}}(\tau)$ in (47) can be computed as

$$\begin{aligned} \nabla_{\tau} J_{\text{SAA}}(\tau) &= \partial_{\tau} L_{\text{SAA}}((u_m)_{m=1}^M, (v_m)_{m=1}^M; (\zeta_m)_{m=1}^M, \tau) \\ &= \beta_P \nabla_{\tau} P(\tau) + \sum_{m=1}^M \partial_{\tau} A(u_m, v_m; \zeta_m, \tau) - \partial_{\tau} F(v_m; \zeta_m, \tau). \end{aligned} \quad (51)$$

Hence, M forward Helmholtz problems in (46) are solved to compute $J_{\text{SAA}}(\tau)$, and M adjoint problems (49) are solved to compute its τ -gradient.

4.3. τ -gradient for the quadratic Taylor approximation

With the quadratic Taylor approximation of the design objective $T_2 Q$, the objective functional (13) becomes

$$J_{T_2}(\tau) = Q(u) + \frac{1}{2} \sum_{n=1}^N \lambda_n + \beta_V \left(\langle \bar{g}, C\bar{g} \rangle + \frac{1}{2} \sum_{n=1}^N \lambda_n^2 \right) + \beta_P P(\tau), \quad (52)$$

where the τ -gradient \bar{g} is given by (34). Then the optimization problem (16) reads

$$\min_{\tau \in \mathcal{Z}} J_{T_2}(\tau) \quad (53)$$

subject to

$$\begin{aligned} A(u, \tilde{v}; \bar{\zeta}, \tau) &= F(\tilde{v}; \bar{\zeta}, \tau) \quad \forall \tilde{v} \in V, \\ A(\tilde{u}, v; \bar{\zeta}, \tau) &= -\langle \partial_u Q(u), \tilde{u} \rangle \quad \forall \tilde{u} \in V, \\ A(\hat{u}_n, \tilde{v}; \bar{\zeta}, \tau) &= -\langle \partial_{\zeta} A(u, \tilde{v}; \bar{\zeta}, \tau) + \partial_{\zeta} F(\tilde{v}; \bar{\zeta}, \tau), \psi_n \rangle, \quad \forall \tilde{v} \in V, n = 1, \dots, N, \\ A(\tilde{u}, \hat{v}_n; \bar{\zeta}, \tau) &= -\langle \partial_{uu} Q(u) \hat{u}_n, \tilde{u} \rangle - \langle \partial_{\zeta} A(\tilde{u}, v; \bar{\zeta}, \tau), \psi_n \rangle \quad \forall \tilde{u} \in V, n = 1, \dots, N, \\ \langle \tilde{\mathcal{H}} \psi_n, \phi \rangle &= \langle \lambda_n C^{-1} \psi_n, \phi \rangle \quad \forall \phi \in X, n = 1, \dots, N, \\ \langle C^{-1} \psi_n, \psi_m \rangle &= 1, \quad m, n = 1, \dots, N, \end{aligned} \quad (54)$$

which correspond to the forward Helmholtz equation (32), the adjoint Helmholtz equation (33), the incremental forward Helmholtz equation (36) for $\hat{\zeta} = \psi_n, n = 1, \dots, N$, the incremental adjoint Helmholtz equation (37) for $\hat{\zeta} = \psi_n, n = 1, \dots, N$, the generalized eigenvalue problem (28) for the eigenpairs (λ_n, ψ_n) , where the τ -Hessian action $\tilde{\mathcal{H}} \psi_n$ is given by (38), $n = 1, \dots, N$,

and the orthonormality condition (29) for the eigenfunctions ψ_n , $n = 1, \dots, N$. As can be seen, the dominant cost of computing the objective functional $J_{T_2}(\tau)$ is N pairs of (incremental) forward/adjoint Helmholtz equations. This is in contrast with the M forward Helmholtz equations which must be solved to compute the SAA objective J_{SAA} .

To compute the τ -gradient of the approximate objective functional (53) with the PDE constraints (54), we form the Lagrangian

$$\begin{aligned}
L_{T_2}(u, v, (\hat{u}_n)_{n=1}^N, (\hat{v}_n)_{n=1}^N, (\lambda_n)_{n=1}^N, (\psi_n)_{n=1}^N, \\
u^*, v^*, (\hat{u}_n^*)_{n=1}^N, (\hat{v}_n^*)_{n=1}^N, (\lambda_{m,n}^*)_{m,n=1}^N, (\psi_n^*)_{n=1}^N, \tau) \\
= J_{T_2}(\tau) \\
+ A(u, v^*; \bar{\zeta}, \tau) - F(v^*; \bar{\zeta}, \tau) \\
+ A(u^*, v; \bar{\zeta}, \tau) + \langle \partial_u Q(u), u^* \rangle \\
+ \sum_{n=1}^N A(\hat{u}_n, \hat{v}_n^*; \bar{\zeta}, \tau) + \langle \partial_\zeta A(u, \hat{v}_n^*; \bar{\zeta}, \tau) + \partial_\zeta F(\hat{v}_n^*; \bar{\zeta}, \tau), \psi_n \rangle \\
+ \sum_{n=1}^N A(\hat{u}_n^*, \hat{v}_n; \bar{\zeta}, \tau) + \langle \partial_{uu} Q(u) \hat{u}_n, \hat{u}_n^* \rangle + \langle \partial_\zeta A(\hat{u}_n^*, v; \bar{\zeta}, \tau), \psi_n \rangle \\
+ \sum_{n=1}^N \langle \bar{\mathcal{H}} \psi_n, \psi_n^* \rangle - \langle \lambda_n C^{-1} \psi_n, \psi_n^* \rangle \\
+ \sum_{m,n=1}^N \lambda_{m,n}^* (\langle C^{-1} \psi_n, \psi_m \rangle - \delta_{mn}).
\end{aligned} \tag{55}$$

By setting the variation of this Lagrangian with respect to λ_n to zero, we obtain

$$\psi_n^* = \frac{1 + 2\beta_V \lambda_n}{2} \psi_n, \quad n = 1, \dots, N. \tag{56}$$

By setting the variation with respect to \hat{v}_n to zero, we have: find $\hat{u}_n^* \in V$ such that

$$A(\hat{u}_n^*, \tilde{v}; \bar{\zeta}, \tau) = -\langle \partial_\zeta A(u, \tilde{v}; \bar{\zeta}, \tau) - \partial_\zeta F(\tilde{v}; \bar{\zeta}, \tau), \psi_n^* \rangle \quad \forall \tilde{v} \in V, \tag{57}$$

which has the same form as the incremental forward Helmholtz equation (36), so that by (56) we have

$$\hat{u}_n^* = \frac{1 + 2\beta_V \lambda_n}{2} \hat{u}_n, \quad n = 1, \dots, N. \tag{58}$$

Similarly, by setting the variation of L_{T_2} with respect to \hat{u}_n to zero, we have: find $\hat{v}_n^* \in V$ such that

$$A(\tilde{u}, \hat{v}_n^*; \bar{\zeta}, \tau) = -\langle \partial_{uu} Q(u) \tilde{u}, \hat{u}_n^* \rangle - \langle \partial_\zeta A(\tilde{u}, v; \bar{\zeta}, \tau), \psi_n^* \rangle \quad \forall \tilde{u} \in V, \tag{59}$$

which has the same form as the incremental adjoint Helmholtz equation (37), so that by (56) and (58) we have

$$\hat{v}_n^* = \frac{1 + 2\beta_V \lambda_n}{2} \hat{v}_n, \quad n = 1, \dots, N. \tag{60}$$

Then, by setting the variation of L_{T_2} with respect to v to zero, we obtain: find $u^* \in V$ such that

$$\begin{aligned}
A(u^*, \tilde{v}; \bar{\zeta}, \tau) = & -2\beta_V \langle \partial_\zeta A(u, \tilde{v}; \bar{\zeta}, \tau) - \partial_\zeta F(\tilde{v}; \bar{\zeta}, \tau), C\bar{g} \rangle \\
& - \langle \partial_\zeta A(\hat{u}_n^*, \tilde{v}; \bar{\zeta}, \tau), \psi_n \rangle - \langle \partial_\zeta A(\hat{u}_n, \tilde{v}; \bar{\zeta}, \tau), \psi_n^* \rangle \\
& - \langle \partial_{\zeta\zeta} A(u, \tilde{v}; \bar{\zeta}, \tau) \psi_n - \partial_{\zeta\zeta} F(\tilde{v}; \bar{\zeta}, \tau) \psi_n, \psi_n^* \rangle \quad \forall \tilde{v} \in V.
\end{aligned} \tag{61}$$

Finally, by setting the variation of L_{T_2} with respect to u to zero, we obtain: find $v^* \in V$ such that

$$\begin{aligned} A(\tilde{u}, v^*; \bar{\zeta}, \tau) &= -\langle \partial_u Q(u), \tilde{u} \rangle - 2\beta_V \langle \partial_{\zeta} A(\tilde{u}, v; \bar{\zeta}, \tau), C\bar{g} \rangle \\ &\quad - \langle \partial_{uu} Q(u) u^*, \tilde{u} \rangle - \langle \partial_{\zeta} A(\tilde{u}, \hat{v}_n^*; \bar{\zeta}, \tau), \psi_n \rangle \\ &\quad - \langle \partial_{\zeta} A(\tilde{u}, \hat{v}_n; \bar{\zeta}, \tau) + \partial_{\zeta\zeta} A(\tilde{u}, v; \bar{\zeta}, \tau) \psi_n, \psi_n^* \rangle \quad \forall \tilde{u} \in V. \end{aligned} \quad (62)$$

Note that the design variable τ is not involved in the orthonormality condition of the eigenfunctions, so there is no need to compute $\lambda_{m,n}^*$ in the Lagrangian. With all the other Lagrange multipliers available, we can compute the τ -gradient as

$$\begin{aligned} \nabla_{\tau} J_{T_2}(\tau) &= \partial_{\tau} L(u, v, (\hat{u}_n)_{n=1}^N, (\hat{v}_n)_{n=1}^N, (\lambda_n)_{n=1}^N, (\psi_n)_{n=1}^N, \\ &\quad u^*, v^*, (\hat{u}_n^*)_{n=1}^N, (\hat{v}_n^*)_{n=1}^N, (\lambda_{m,n}^*)_{m,n=1}^N, (\psi_n^*)_{n=1}^N, \tau). \end{aligned} \quad (63)$$

4.4. The approximate Newton algorithm

Once the τ -gradient is computed for the different approximations, and the τ -Hessian action is computed for the deterministic approximation, we can solve the optimization problem by an approximate Newton algorithm with backtracking line search to guarantee monotonic convergence, where the τ -Hessian is computed or approximated by the τ -Hessian of the deterministic approximation, and the resulting linear system is solved by inexact preconditioned conjugate gradient method with Steihaug's stopping criteria.

Algorithm 2 Line search inexact approximate Newton-pCG algorithm

Input: the maximum numbers of approximate Newton, CG, and line search iterations N_{qn} , N_{cg} , N_{ls} , and the convergence tolerance ϵ_{qn} for the approximate Newton.

Output: solution of the optimization problem τ^* .

1. Initialize a design variable τ_0 , set $n_{qn}, n_{cg}, n_{ls} = 0$, set the tolerance $\epsilon_{qn} = 2\epsilon_{qn}$, set the tolerance for CG convergence to $\epsilon_{cg} = \epsilon_{cg}^0$.

while $n_{qn} < N_{qn}$ and $\epsilon_{qn} < \epsilon_{qn}$ **do**

2. Solve the Newton linear system: find the update direction $\delta\tau \in Z$ by solving

$$\nabla_{\tau}^2 J_{\bar{\zeta}}(\tau_{n_{qn}}) \delta\tau = -\nabla_{\tau} J_a(\tau_{n_{qn}}) \quad (64)$$

using a CG method with preconditioner $\beta_P \nabla_{\tau}^2 P(\tau)$, terminated by Steihaug's criteria, namely, when $n_{cg} \geq N_{cg}$, or $\epsilon_{cg} \geq \epsilon_{cg}$, or $\langle \nabla_{\tau}^2 J_{\bar{\zeta}}(\tau_{n_{qn}}) \delta\tau, \delta\tau \rangle < 0$ (i.e., when a direction of negative curvature is encountered).

while $J_a(\tau_{n_{qn}} + \alpha\delta\tau) > J_a(\tau_{n_{qn}}) + c_{AG}\alpha\delta\tau$ and $n_{ls} < N_{ls}$ **do**

3. Set $\alpha = 2^{-n_{ls}}$ and compute $J_a(\tau_{n_{qn}} + \alpha\delta\tau)$. Set $n_{ls} \leftarrow n_{ls} + 1$.

end while

4. Break the while loop if $n_{ls} \geq N_{ls}$.

5. Set $\tau_{n_{qn}+1} = \tau_{n_{qn}} + \alpha\delta\tau$, $n_{qn} \leftarrow n_{qn} + 1$, $n_{cg}, n_{ls} = 0$, compute ϵ_{qn} , and update the tolerance for CG convergence at $\epsilon_{cg} = \min\{\epsilon_{cg}^0, \|\nabla J_a(\tau_{n_{cg}})\|/\|\nabla J_a(\tau_0)\|\}$.

end while

6. Set $\tau^* = \tau_{n_{qn}}$.

The method is summarized in Algorithm Algorithm 2. In (64) of Algorithm 2, J_a represents the approximation of the objective functional $J \approx J_a$, with the deterministic approximation $J_a =$

$J_{\bar{\zeta}}$, the sample average approximation $J_a = J_{\text{SAA}}$, and the Taylor approximation $J_a = J_{T_2}$. For the sample average approximation and Taylor approximation, the τ -Hessian of J_a is approximated by the τ -Hessian of the deterministic approximation $\nabla_{\tau}^2 J_{\bar{\zeta}}$ given by (45), while the gradients are computed as in Sections 4.1, 4.2, and 4.3 for the deterministic, SAA, and Taylor approximations, respectively. For the termination condition in step $n_{qn} + 1$ of the approximate Newton iteration, we can use a quantity related to the norm of the gradient $\|\nabla_{\tau} J_a(\tau_{n_{qn}})\|$ and/or $\langle \nabla_{\tau} J_a(\tau_{n_{qn}}), \delta\tau \rangle$. c_{AG} is a small constant for Armijo–Goldstein conditions, e.g., $c_{\text{AG}} = 10^{-4}$.

In each of the approximate Newton iteration, we have to compute once the τ -gradient $\nabla_{\tau} J_a$, perform n_{cg} τ -Hessian actions, i.e., the actions of $\nabla_{\tau}^2 J_{\bar{\zeta}}$ in given CG directions while solving (64), which requires solution of a pair of incremental forward/adjoint Helmholtz equations (43) and (44) for each Hessian action, as well as n_{ls} backtracking line search iterations, which requires n_{ls} evaluations of J_a . For relatively small uncertainty, i.e., small signal-to-noise level, we expect that the Hessian $\nabla_{\tau}^2 J_{\bar{\zeta}}$ is a good approximation of $\nabla_{\tau}^2 J_a$, and the total number of Newton iterations n_{qn} is independent of the dimension of the discretized design variable field. Moreover, the number of preconditioned CG iterations n_{cg} is also expected to be independent of the design variable dimension when the τ -Hessian of the approximation for $\mathbb{E}[Q] + \beta_V \text{Var}[Q]$ is low-rank. Therefore, the inexact approximate Newton–pCG algorithm is expected to be scalable with respect to the dimension of the design variable τ , in the sense that the number of Helmholtz solves will be independent of the design variable dimension. This will be demonstrated numerically in Section 5.3.

5. Numerical experiments

In this section, we present several numerical experiments to: (1) demonstrate the effectiveness of the optimization strategy in a deterministic setting, (2) compare the difference between various approximation methods for the optimization under uncertainty, (3) illustrate the scalability of the Taylor approximation and the approximate Newton–pCG algorithm with respect to the dimension of the discretized random variable and design variable fields, respectively, (4) show that the proposed optimization strategy can achieve cloaking for incident waves with multiple directions and multiple frequencies under uncertainty, and finally (5) elucidate the applicability of the proposed optimization strategy to more complex geometries beyond disks.

5.1. Cloaking in a deterministic setting

In this experiment, we aim to demonstrate the effectiveness of the optimization strategy in designing a cloak that makes the obstacle invisible to acoustic waves. In what follows, we use normalized units for all quantities. The configuration of the design problem is displayed in Fig. 1, where the obstacle is a disk of radius $r_1 = 1$, which is surrounded by the cloaking region with radius $r_2 = 3$, and immersed in a host square medium of size $[-6, 6]^2$ with PML boundaries of length 1 on all sides. The incident wave is a plane wave propagating from the left side to the right side, given by $u^{\text{inc}} = e^{ik_0 x \cdot b}$ with direction $b = (1, 0)$ and wavenumber $k_0 = \omega/c_0$ with frequency $\omega = 2\pi$ and sound speed $c_0 = 1$. For this experiment we do not consider uncertainty in the optimal design and fix the random variable at its mean $\zeta = \bar{\zeta} = 0$ in (10). This approach is equivalent to the deterministic approximation presented in Section 3.1. For the regularization of the design variable, we set $\beta_P = 10^{-2}$ in the objective functional (39). A finite element method is used to solve the scattering problem, with mesh of triangles with 172,803 vertices, leading to 345,606, 34,217, and 57,462 degrees of freedom for the discrete state variable (using piecewise

linear elements), the discrete random variable (piecewise linear elements), and the discrete design variable (piecewise constant elements), respectively.

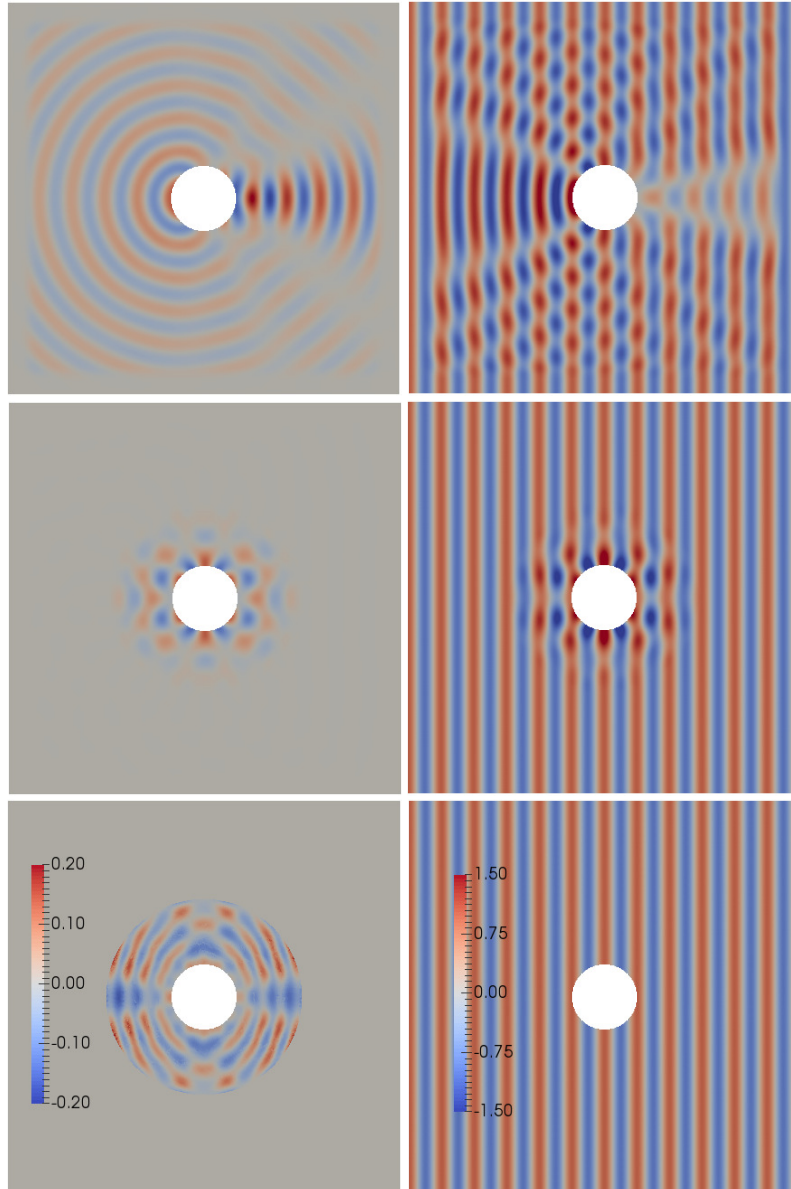


Figure 2: Top: wave scattering from an impenetrable obstacle; left: scattered wave field; right: total wave field. Middle: wave scattering with the optimized cloak; left: scattered wave field; right: total wave field. Bottom, left: the optimal design variable field τ^* obtained by the deterministic optimization; right: the incident wave field, i.e., total wave field in homogeneous medium. The real part of all wave fields are shown.

We initialize the design variable $\tau = 0$ in (10) and run the approximate Newton algorithm as presented in Algorithm 2 to minimize the objective functional (39) with respect to the design variable τ , with $N_{qn} = 10$, $N_{cg} = 10$, $N_{ls} = 10$, and $\varepsilon_{qn} = 10^{-2}$. The algorithm converged in 6 iterations. The results are shown in Fig. 2 with the real part of the scattered and total wave fields shown in the top two images, in which the reflection of the incident wave from the impenetrable obstacle without the cloak is evident. In the middle two images, the scattered and total wave fields are displayed with the cloak at the optimal design. From the middle-left image, we can see a clear reduction of the scattered wave in the observation region—which is essentially invisible outside the cloak region. Inside the cloak region, the scattered wave fields is significantly altered from that without the cloak. From the middle-right images of the total wave field, we can observe an effective cloaking of the obstacle, i.e., the total field coincides with the incident field outside the design region as shown in the bottom-right image. All wave fields are scaled to the range $[-1.5, 1.5]$ for the sake of visual comparison. The optimal design variable τ^* is shown in the bottom-left image, from which we can see a sub-wavelength structure within the cloak, which effectively eliminates the scattered wave in the background medium rendering it undetectable to an external observer. It is worth noting some similarity in the cloaking structure between this approach, which permits continuously varying material properties are possible, and the cloaks constructed from distributions of discrete scatterers reported in references [27, 30, 28].

5.2. Cloaking under uncertainty

In this experiment, we compare the optimal cloaking performance under uncertainty by the three approximation methods presented in Section 3. This uncertainty, due to manufacturing errors or variability in material properties, is modeled as an additive Gaussian random field $\mathcal{N}(\bar{\zeta}, C)$ with the covariance operator $C = (-\gamma\Delta + \delta I)^{-2}$. We take $\gamma = 10$ and $\delta = 50$ such that the noise-to-signal ratio of the random variable is about 20% of the design variable. Two samples of the random (field) variable are shown in Fig. 3.

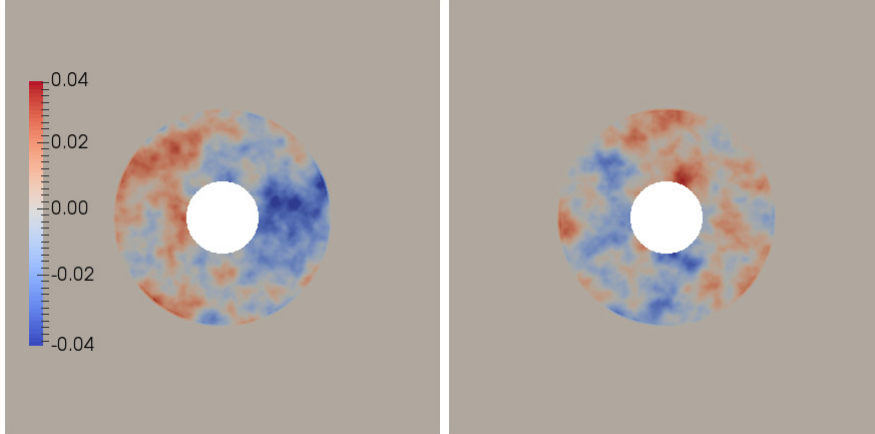


Figure 3: Random samples of $\zeta \sim \mathcal{N}(\bar{\zeta}, C)$ with $\bar{\zeta} = 0$, and $\gamma = 10, \delta = 50$ for $C = (-\gamma\Delta + \delta I)^{-2}$.

The optimal design variables obtained by using different approximations of the objective functional are shown in Fig. 4. We use 50 eigenvalues in the trace estimate (30) for the quadratic

approximation, which achieves about 99% accuracy (shown in the next section). One hundred samples are used for the sample average approximation, which requires similar computational cost as the quadratic approximation. Slight differences can be noticed even though they share the same topological structure.

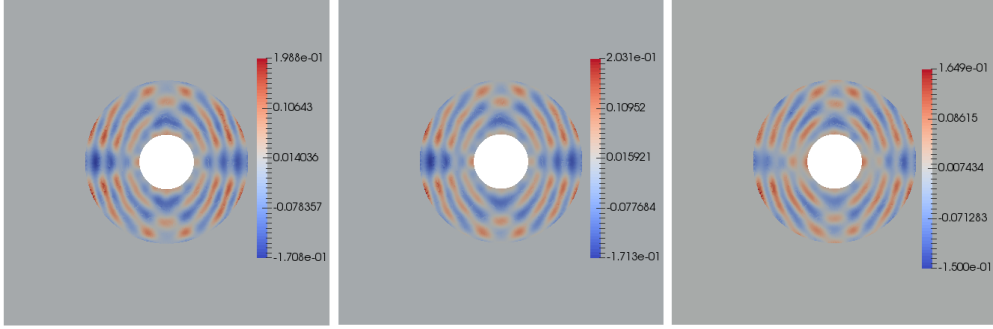


Figure 4: Optimal design variable field τ^* obtained by using deterministic (left), quadratic (middle), and sample average (right) approximations of the objective functional.

We next draw 10 random samples of the random variable ζ , and solve the scattering problem for each optimal design field. The mean and standard deviation of the scattered fields for the 10 random samples are shown in Fig. 5. We can observe that the sample average approximation leads to a more biased scattered field (as seen from its large mean), while the deterministic approximation gives rise to large variation of the scattered field (as seen from its large standard deviation).

Table 1: Estimates \hat{Q} of the design objective Q and mean squared errors (MSE) for \hat{Q} , $Q - T_1Q$, and $Q - T_2Q$, based on 10 samples for a random design τ_{random} , the deterministic optimal design τ_{deter} , and the optimal design under uncertainty using the quadratic τ_{quad} and the sample average τ_{saa} approximations.

design	\hat{Q}	MSE(\hat{Q})	MSE($Q - T_1Q$)	MSE($Q - T_2Q$)
τ_{random}	1.19E+01	8.34E-02	4.50E-03	4.89E-05
τ_{deter}	1.39E+00	5.47E-02	5.47E-02	1.48E-04
τ_{quad}	8.28E-01	2.37E-02	1.62E-02	3.56E-05
τ_{saa}	2.00E+00	8.40E-03	2.30E-02	5.66E-05

To assess the accuracy of the Taylor approximation, we compute the mean squared errors (MSE) of the the design objective Q and its residual using the linear and quadratic (T_2) Taylor approximations, as well as the quantity $q = (Q - Q(\bar{\zeta}))^2$ in the evaluation of the variance. The results are obtained at a random design, and the optimal design with deterministic, quadratic Taylor, and sample average approximations, and are shown in Table 1 and 2. These results indicate that the quadratic approximation is much more accurate than the linear approximation, both achieving errors smaller than 1%. We further remark that if higher accuracy is required, we can use the quadratic approximation as a control variate to reduce the variance in a sample average approximation, as introduced in [9].

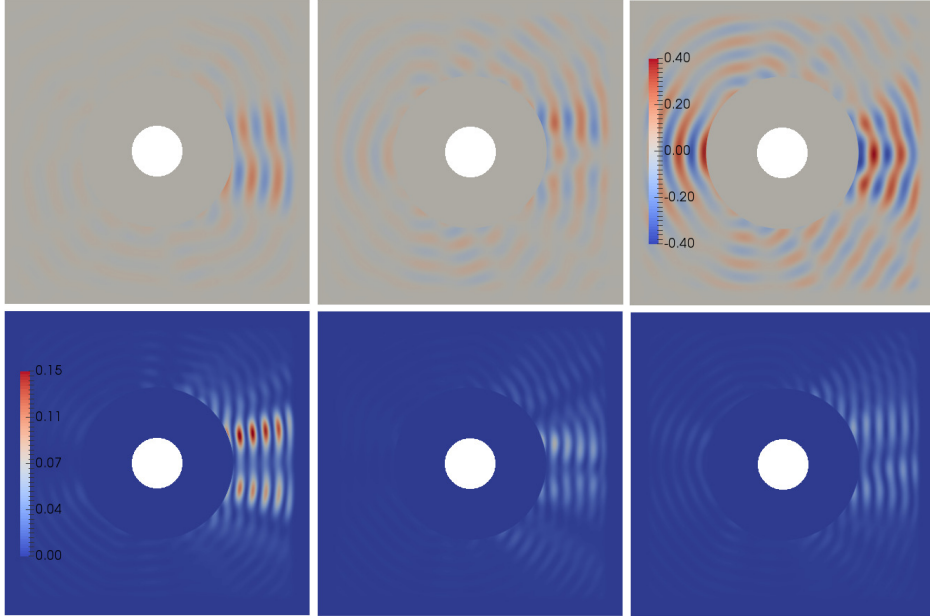


Figure 5: Mean (top) and standard deviation (bottom) of the scattered wave field at the optimal design τ^* obtained by using deterministic (left), quadratic (middle), and sample average (right) approximations of the objective functional.

Table 2: Estimates \hat{q} of $q = (Q - Q(\bar{\zeta}))^2$ and mean squared errors (MSE) for \hat{q} , $q - T_1q$, and $q - T_2q$ based on 10 samples for a random design τ_{random} , the deterministic optimal design τ_{deter} , and the optimal design under uncertainty using the quadratic τ_{quad} and the sample average τ_{saa} approximations.

design	\hat{q}	$\text{MSE}(\hat{q})$	$\text{MSE}(q - T_1q)$	$\text{MSE}(q - T_2q)$
τ_{random}	1.42E+02	4.83E+01	2.29E+00	3.24E-02
τ_{deter}	2.48E+00	7.49E-01	7.49E-01	3.92E-03
τ_{quad}	9.22E-01	1.07E-01	9.04E-02	2.53E-04
τ_{saa}	4.08E+00	1.46E-01	2.48E-01	1.06E-03

5.3. Scalability of the approximation and optimization methods

The random variable and the design variable are spatially distributed functions, whose dimensions can be very high after discretization. It is therefore crucial that the approximation and optimization are scalable with respect to both random and design variables. To illustrate the scalability of the approximation and optimization methods, we use a sequence of refined meshes as reported in Table 3, which correspond to a sequence of increased dimensions for the random and design variables.

As shown in Fig. 6, the scalability with respect to the complexity of the quadratic approximation is implied by the similar decay pattern of the absolute eigenvalues of the generalized eigenvalue problem (28) across the refined meshes, which determines the accuracy of the trace estimate. Moreover, the accuracy of the quadratic approximation measured by the mean squared

Table 3: Degrees of freedom (DOF) for finite element discretization of the state variable u and random variable ζ with piecewise linear elements (P1), and design variable τ with piecewise constant elements (P0), at a sequence of (uniformly refined) meshes, denoted by meth1, meth2, meth3, meth4, meth5.

DOF	mesh1	mesh2	mesh3	mesh4	mesh5
$u(\text{P1})$	22,110	86,788	345,606	1,373,814	5,488,216
$\zeta(\text{P1})$	2,347	8,795	34,217	134,796	535,321
$\tau(\text{P0})$	4,454	17,114	67,462	267,640	1,066,761

errors is reported in Table 4 and 5, which remains about 1% with increasing dimensions, and indicates that the accuracy of the quadratic approximation is also scalable.

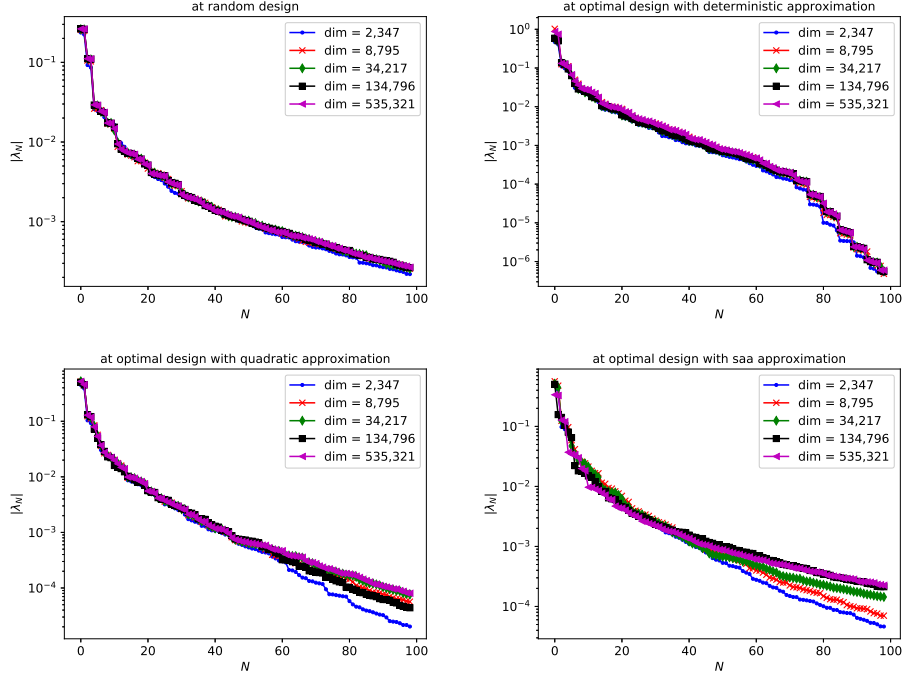


Figure 6: Decay of the absolute generalized eigenvalues of the covariance preconditioned Hessian in (28) at different designs. A design at a realization of space white noise (top-left); the optimal design obtained with deterministic (top-right), quadratic (bottom-left), and sample average approximations (bottom-right).

As for the scalability of the approximate Newton optimization algorithm, we plot the decay of the objective functional against the number of optimization iterations in Fig. 7. Fast and relatively mesh-independent decay of the objective functional can be observed for the deterministic approximation, which is understandable since the Hessian approximation in Section 4.1 is in fact exact in this case, so that the method is a proper Newton method. For the quadratic approximation, convergence is only weakly dependent on the discretization (with sufficient mesh

Table 4: Estimates \hat{Q} of the design objective Q and mean squared errors (MSE) for \hat{Q} , $Q - T_1Q$, and $Q - T_2Q$, based on 10 samples for different parameter dimensions.

dimension	\hat{Q}	MSE(\hat{Q})	MSE($Q - T_1Q$)	MSE($Q - T_2Q$)
2,347	6.49E-01	1.28E-02	8.92E-03	1.01E-04
8,795	7.66E-01	1.66E-02	1.07E-02	1.54E-04
34,217	8.28E-01	2.37E-02	1.62E-02	3.56E-05

Table 5: Estimates \hat{q} of $q = (Q - Q(\tilde{\zeta}))^2$ and mean squares errors (MSE) \hat{q} , $q - T_1q$, and $q - T_2q$, based on 10 samples for different parameter dimensions.

dimension	\hat{q}	MSE(\hat{q})	MSE($q - T_1q$)	MSE($q - T_2q$)
2,347	5.49E-01	3.42E-02	3.28E-02	5.61E-04
8,795	7.54E-01	9.00E-02	7.39E-02	1.64E-03
34,217	9.22E-01	1.07E-01	9.04E-02	2.53E-04

resolution); thus the use of the deterministic Hessian in place of the true Hessian still results in a relatively scalable number of optimization iterations. In contrast, the use of the deterministic Hessian for the sample average approximation does not yield a scalable method in this case, as shown by the dependence of the iterations on mesh size and the resulting problem dimension.

5.4. Multiple directions and multiple frequencies

In this numerical experiment, we assess the ability of the optimal cloak to hide the obstacle from the incident wave from multiple attack angles and multiple frequencies. In the test, for the incident wave $e^{ikx \cdot b}$ we choose four attack angles, $b = (1, 0), (0, 1), (0, -1), (-1, 0)$, and four frequencies $k = k_0/2, 2k_0/3, 5k_0/6, k_0$, and set three test trials. In the first trial, we use four directions at one frequency $k = k_0$; in the second trial, we use four frequencies at one direction $b = (1, 0)$; in the third trial, we use four directions at four frequencies $b = (1, 0), (0, 1), (0, -1), (-1, 0)$ and $k = k_0/2, 2k_0/3, 5k_0/6, k_0$.

The optimal design under uncertainty using the quadratic approximation for the three different settings is shown in Fig. 8, from which we can observe distinct patterns. The real parts of the total wave without and with the cloak are shown in Fig. 9 – 11. We observe that the cloak can achieve effective cloaking for different directions with the same frequency, and can effectively reduce the scattering for different frequencies. This is expected as the characteristic length of the cloak has to accommodate all different wavelengths.

5.5. Toward more complex geometry

Finally, we demonstrate the applicability of the proposed optimization method for an obstacle with more complex geometry (notionally a stealth aircraft) as shown in Fig. 12. The design variable field is discretized by a spatially-adapted mesh with 451,376 vertices and 898,136 elements, which results in DOF of 902,752 for the discrete state variable field with piecewise linear elements in the entire domain, 101,535 for the discrete uncertain variable field with piecewise

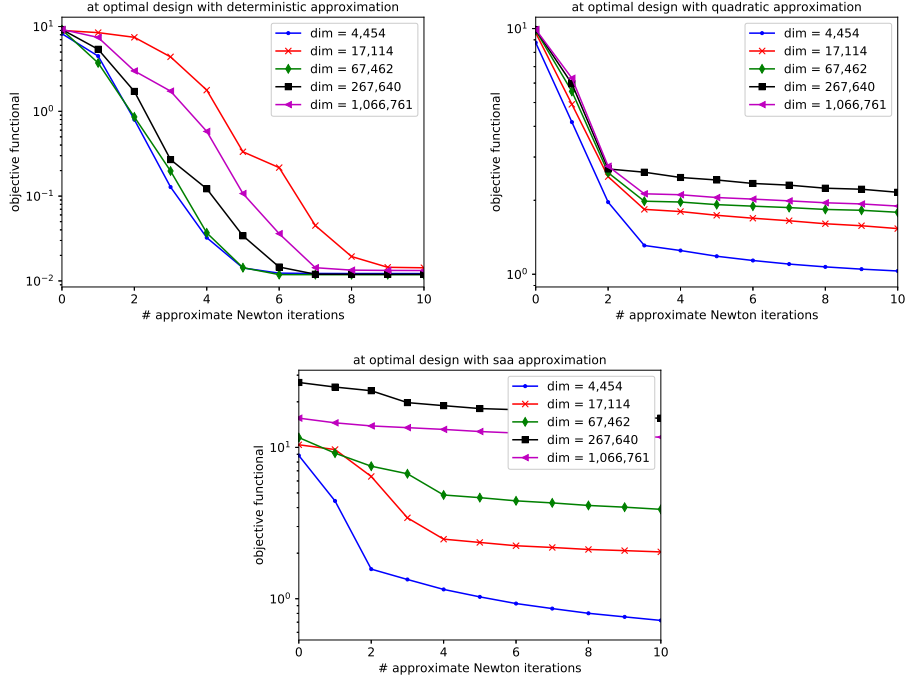


Figure 7: Decay of the objective functional with the number of approximate Newton optimization steps for deterministic approximation (top-left), quadratic approximation (top-right), and sample average approximation (bottom).

linear elements in the thin cloaking layer (shown in yellow), and 196,238 for the discrete optimization variable field with piecewise constant elements in the thin cloaking layer. We restrict ourselves to solution of the deterministic optimal cloak problem, in order to demonstrate the feasibility of computing the Hessian—which is a critical ingredient for the approximate Newton method—for such a large problem. Fig. 13 shows the large reduction in the scattered wave field achieved after 200 iterations of the optimization method. The reduction in the scattered field is striking, considering the thinness of the cloak region and sharp corners.

6. Conclusions

In this paper, we have developed a simulation-based optimal design strategy for acoustic cloaks in the presence of material property uncertainty. To the best of our knowledge this is the first work that takes into account uncertainty in a systematic way for optimal design of an acoustic cloak that is robust to material variability and manufacturing error. Both the design variables and the uncertain parameters are modeled by infinite-dimensional spatially-varying fields, which become high-dimensional upon faithful discretization of the optimal design problem. To tackle the curse of dimensionality in the approximation of the uncertain parameter field, we employed a scalable approximation method of the mean-variance objective based on a Taylor expansion and a randomized SVD algorithm. To solve the resulting high-dimensional optimization problem,

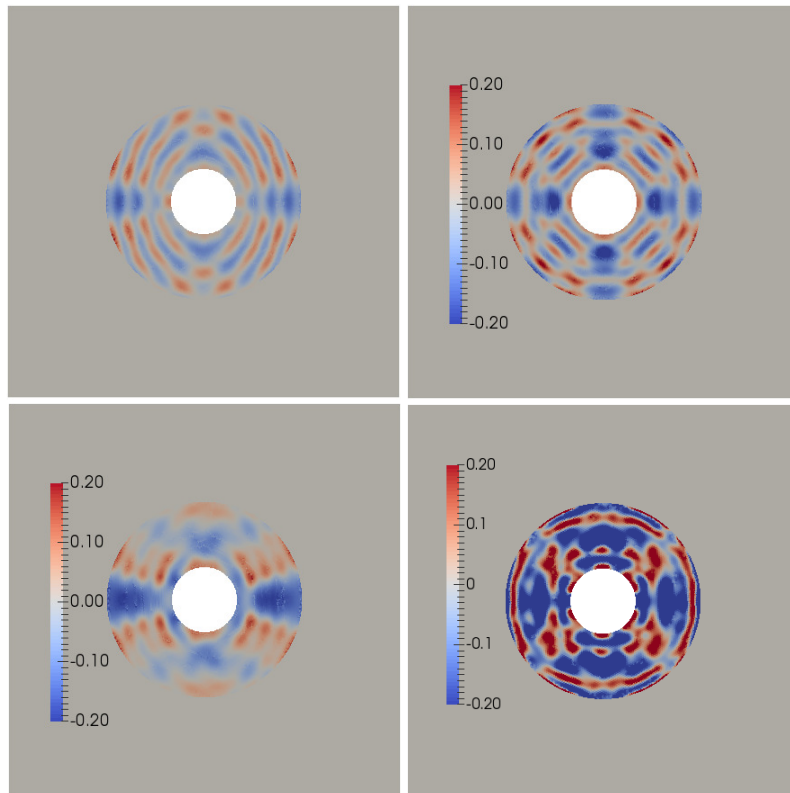


Figure 8: Optimal designs under uncertainty using quadratic approximation. One direction and one frequency (top-left), which is the same as in Fig. 4, four directions and one frequency (top-right), one direction and four frequencies (bottom-left), and four directions and four frequencies (bottom-right).

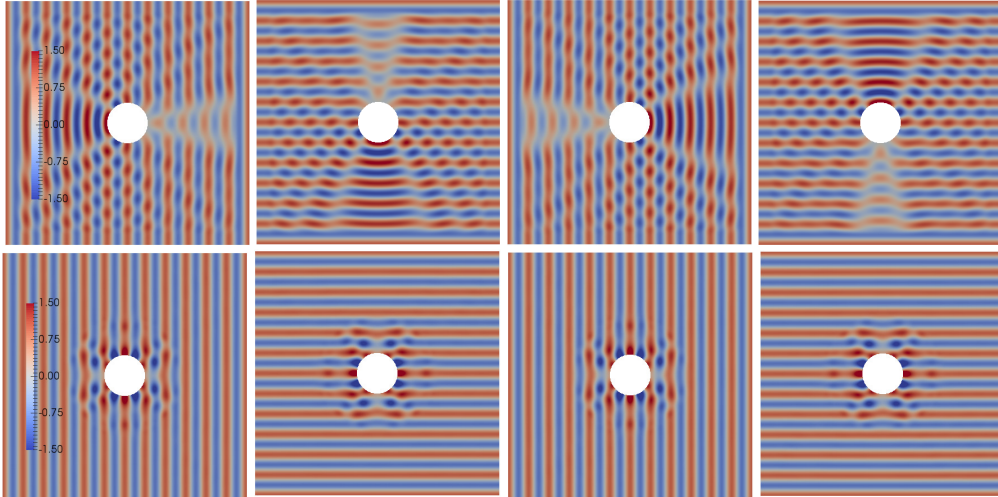


Figure 9: The real part of the total wave fields without (top) and with (bottom) the cloak designed under uncertainty for the case of four directions and one frequency.

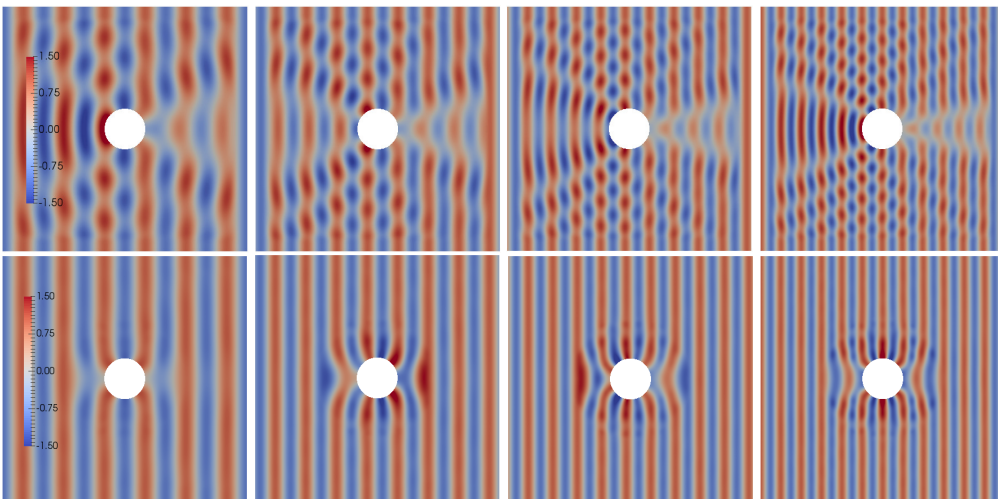


Figure 10: The real part of the total wave fields without (top) and with (bottom) the cloak designed under uncertainty for the case of one direction and four frequencies.

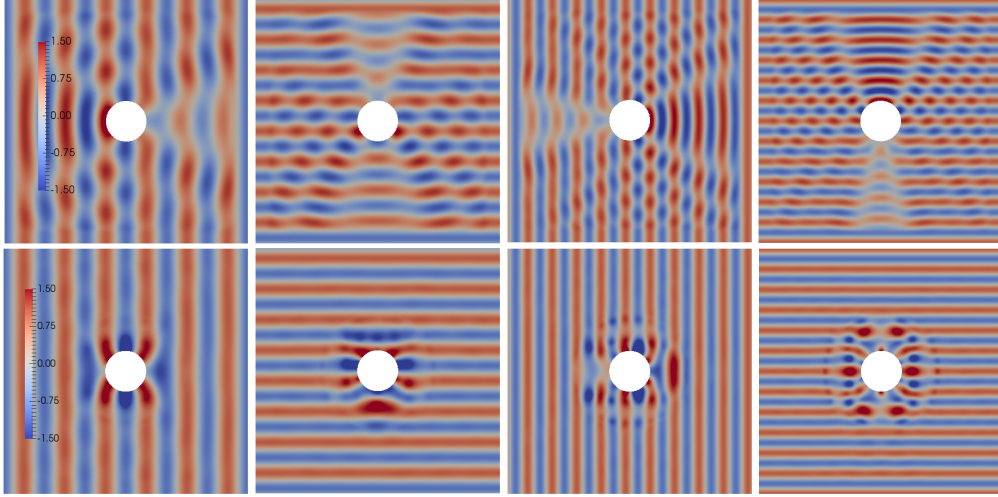


Figure 11: The real part of the total wave fields without (top) and with (bottom) the cloak designed under uncertainty for the case of four directions and four frequencies.

we developed an approximate Newton method in which the Hessian of the deterministic approximation of the objective functional is used to provide an effective approximation of the Hessian of the Taylor approximation of the objective functional, motivated by the moderate uncertainty due to material variability.

We demonstrated that the optimal design effectively eliminates the scattered wave field from waves incident on simple circular scatterers, not only for a single direction and single frequency, but also for multiple-direction and multiple-frequency waves. We also demonstrated that the deterministic optimization problem, on which the approximate Hessian for the optimization under uncertainty problem is based, can be tractably computed for an obstacle with complex geometry. Moreover, we showed that the optimal design under uncertainty performs better (lower variance in the scattered wave field) in the case of random material properties than a deterministic design does.

The proposed methodology is essentially scalable with respect to increasing dimensions of design variables and uncertain parameters as numerically evidenced by: the small and dimension-independent number of forward Helmholtz solves needed to evaluate the Taylor-approximated objective function; the weak dependence of the optimization iterations on the problem dimension; and the dimension-independent accuracy of the quadratic Taylor approximation.

Future research directions include (1) adding manufacturability constraints on the design variable field stemming from additive manufacturing processes; (2) considering more complex three-dimensional problems with more general objectives beyond cloaking; (3) developing and applying higher order Taylor approximations (beyond quadratic) [75] for the objective functional for cases where large uncertainties arise; and (4) employing the Taylor approximations as control variates in a variance reduction framework [9].

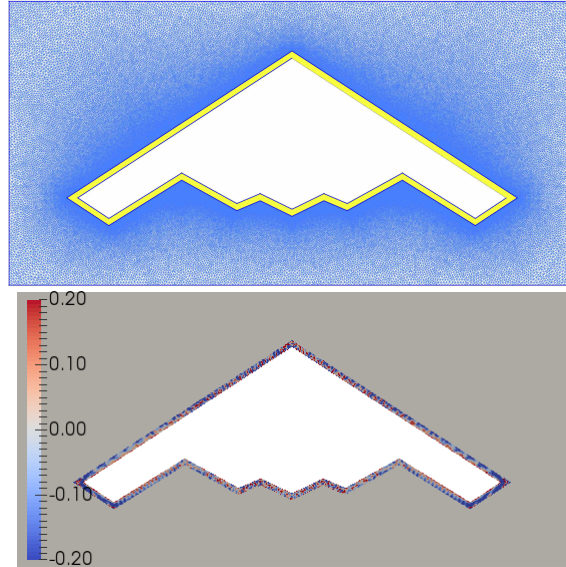


Figure 12: Top: Geometry and adaptive mesh. Bottom: Optimal design field with deterministic approximation

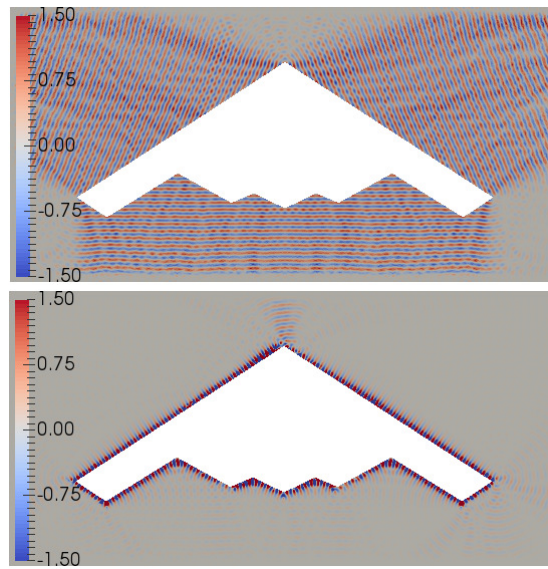


Figure 13: The real part of the scattered wave fields without (top) and with (bottom) the cloak.

References

- [1] M. R. Haberman, M. D. Guild, Acoustic metamaterials, *Physics Today* 69 (2016) 42–48. doi:10.1063/PT.3.3198.
- [2] S. Cummer, J. Christensen, A. Alù, Controlling sound with acoustic metamaterials, *Nature Reviews Materials* 1 (2016) 16001. doi:10.1038/natrevmats.2016.1.
- [3] G. Ma, P. Sheng, Acoustic metamaterials: From local resonances to broad horizons, *Science Advances* 2 (2016) e1501595. doi:10.1126/sciadv.1501595.
- [4] J. Mueller, Parallel total variation minimization, Diploma thesis, University of Muenster, WWU (november 2008).
- [5] J. N. A. Matthews, Mechanical metamaterials roll off the 3d printing press, *Physics Today* 68 (2015) 26.
- [6] M. Wegener, S. Linden, Shaping optical space with metamaterials, *Physics Today* 63 (10) (2010) 32.
- [7] A. Alexanderian, N. Petra, G. Stadler, O. Ghattas, Mean-variance risk-averse optimal control of systems governed by PDEs with random parameter fields using quadratic approximations, *SIAM/ASA Journal on Uncertainty Quantification* 5 (1) (2017) 1166–1192, arXiv preprint arXiv:1602.07592. doi:10.1137/16M106306X.
- [8] A. Alexanderian, P. Gloor, O. Ghattas, On Bayesian A-and D-optimal experimental designs in infinite dimensions, *Bayesian Analysis*.
- [9] P. Chen, U. Villa, O. Ghattas, Taylor approximation and variance reduction for PDE-constrained optimal control under uncertainty, *Journal of Computational Physics* 385 (2019) 163–186.
URL <https://arxiv.org/abs/1804.04301>
- [10] O. Bashir, K. Willcox, O. Ghattas, B. van Bloemen Waanders, J. Hill, Hessian-based model reduction for large-scale systems with initial condition inputs, *International Journal for Numerical Methods in Engineering* 73 (2008) 844–868.
- [11] S. Cummer, *Acoustic metamaterials*, Springer, New York, NY, 2013, Ch. 8, Transformation Acoustics, pp. 197–218.
- [12] H. Chen, C. T. Chan, Acoustic cloaking and transformation acoustics, *Journal of Physics D: Applied Physics* 43 (2010) 113001. doi:10.1088/0022-3727/43/11/113001.
- [13] S. A. Cummer, B.-I. Popa, D. Schurig, D. R. Smith, J. Pendry, M. Rahm, A. Starr, Scattering theory derivation of a 3d acoustic cloaking shell, *Physical Review Letters* 100 (2008) 024301. doi:10.1103/PhysRevLett.100.024301.
- [14] A. N. Norris, Acoustic cloaking theory, *Proceedings of the Royal Society of America A* 464 (2008) 2411 – 2434.
- [15] D. Torrent, J. Sánchez-Dehesa, Acoustic cloaking in two dimensions: A feasible approach, *New Journal of Physics* 10 (2008) 063015.
URL <http://stacks.iop.org/1367-2630/10/i=6/a=063015>
- [16] S. Zhang, C. Xia, N. Fang, Broadband acoustic cloak for ultrasound waves, *Phys. Rev. Lett.* 106 (2011) 024301. doi:10.1103/PhysRevLett.106.024301.
URL <https://link.aps.org/doi/10.1103/PhysRevLett.106.024301>
- [17] A. Alù, N. Engheta, Achieving transparency with plasmonic and metamaterial coatings, *Physical Review E* 72 (2005) 016623. doi:10.1103/PhysRevE.72.016623.
URL <https://link.aps.org/doi/10.1103/PhysRevE.72.016623>
- [18] D. Rainwater, A. Kerkhoff, K. Melin, J. C. Soric, G. Moreno, A. Alù, Experimental verification of three-dimensional plasmonic cloaking in free-space, *New Journal of Physics* 14 (1) (2012) 013054.
URL <http://stacks.iop.org/1367-2630/14/i=1/a=013054>
- [19] M. D. Guild, M. R. Haberman, A. Alù, Plasmonic cloaking and scattering cancellation for electromagnetic and acoustic waves, *Wave Motion* 48 (2011) 468–482. doi:10.1016/j.wavemoti.2011.02.006.
- [20] M. D. Guild, A. Alù, M. R. Haberman, Cancellation of acoustic scattering from an elastic sphere, *The Journal of the Acoustical Society of America* 129 (2011) 1355–1365. doi:10.1121/1.3552876.
- [21] U. Leonhardt, Optical conformal mapping, *Science* 312 (2006) 1777–1780. doi:10.1126/science.1126493.
- [22] A. Alù, N. Engheta, Cloaking a sensor, *Physical Review Letters* 102 (2009) 233901. doi:10.1103/PhysRevLett.102.233901.
URL <https://link.aps.org/doi/10.1103/PhysRevLett.102.233901>
- [23] A. Alù, N. Engheta, Cloaked near-field scanning optical microscope tip for noninvasive near-field imaging, *Physical Review Letters* 105 (2010) 263906. doi:10.1103/PhysRevLett.105.263906.
URL <https://link.aps.org/doi/10.1103/PhysRevLett.105.263906>
- [24] M. D. Guild, A. Alù, M. R. Haberman, Cloaking an acoustics sensor using scattering cancellation, *Applied Physics Letters* 105 (2014) 023510. doi:10.1063/1.4890614.
- [25] M. D. Guild, M. R. Haberman, A. Alù, Plasmonic-type acoustic cloak made of a bilaminate shell, *Physical Review B* 86 (2012) 104302. doi:10.1103/PhysRevB.86.104302.
URL <https://link.aps.org/doi/10.1103/PhysRevB.86.104302>
- [26] M. D. Guild, A. J. Hicks, M. R. Haberman, A. Alù, P. S. Wilson, Acoustic scattering cancellation of irregular

- objects surrounded by spherical layers in the resonant regime, *Journal of Applied Physics* 118 (2015) 164903. doi:10.1063/1.4933188.
- [27] L. Sanchis, V. M. García-Chocano, R. Llopis-Pontiveros, A. Climente, J. Martínez-Pastor, F. Cervera, J. Sánchez-Dehesa, Three-dimensional axisymmetric cloak based on the cancellation of acoustic scattering from a sphere, *Phys. Rev. Lett.* 110 (2013) 124301. doi:10.1103/PhysRevLett.110.124301. URL <https://link.aps.org/doi/10.1103/PhysRevLett.110.124301>
- [28] Z. Lu, L. Sanchis, J. Wen, L. Cai, Y. Bi, J. Sánchez-Dehesa, Acoustic cloak based on bézier scatterers, *Scientific Reports* 8 (2018) 12924. doi:10.1038/s41598-018-30888-7. URL <https://www.nature.com/articles/s41598-018-30888-7>
- [29] F. A. Amirkulova, A. N. Norris, The gradient of total multiple scattering cross-section and its application to acoustic cloaking, *Journal of Theoretical and Computational Acoustics* (2020) 1950016.
- [30] J. Andkjaer, O. Sigmund, Topology optimized cloak for airborne sound, *Journal of Vibration and Acoustics* 135 (2013) 041011. doi:10.1115/1.4023828. URL <http://dx.doi.org/10.1115/1.4023828>
- [31] A. Borzi, V. Schulz, C. Schillings, G. Von Winckel, On the treatment of distributed uncertainties in PDE-constrained optimization, *GAMM-Mitteilungen* 33 (2) (2010) 230–246.
- [32] C. Schillings, S. Schmidt, V. Schulz, Efficient shape optimization for certain and uncertain aerodynamic design, *Computers & Fluids* 46 (1) (2011) 78–87.
- [33] L. S. Hou, J. Lee, H. Manouzi, Finite element approximations of stochastic optimal control problems constrained by stochastic elliptic PDEs, *Journal of Mathematical Analysis and Applications* 384 (1) (2011) 87–103.
- [34] M. D. Gunzburger, H.-C. Lee, J. Lee, Error estimates of stochastic optimal Neumann boundary control problems, *SIAM Journal on Numerical Analysis* 49 (4) (2011) 1532–1552. doi:10.1137/100801731. URL <http://link.aip.org/link/?SNA/49/1532/1>
- [35] E. Rosseel, G. N. Wells, Optimal control with stochastic PDE constraints and uncertain controls, *Computer Methods in Applied Mechanics and Engineering* 213 (2012) 152–167.
- [36] D. Kouri, D. Heinkenschloos, M. Ridzal, B. Van Bloemen Waanders, A trust-region algorithm with adaptive stochastic collocation for PDE optimization under uncertainty, *SIAM Journal on Scientific Computing* 35 (4) (2012) 1847–1879.
- [37] H. Tiesler, R. M. Kirby, D. Xiu, T. Preusser, Stochastic collocation for optimal control problems with stochastic PDE constraints, *SIAM Journal on Control and Optimization* 50 (5) (2012) 2659–2682.
- [38] P. Chen, A. Quarteroni, G. Rozza, Stochastic optimal Robin boundary control problems of advection-dominated elliptic equations, *SIAM Journal on Numerical Analysis* 51 (5) (2013) 2700–2722.
- [39] T. Lassila, A. Manzoni, A. Quarteroni, G. Rozza, Boundary control and shape optimization for the robust design of bypass anastomoses under uncertainty, *ESAIM: Mathematical Modelling and Numerical Analysis* 47 (4) (2013) 1107–1131.
- [40] P. Chen, A. Quarteroni, Weighted reduced basis method for stochastic optimal control problems with elliptic PDE constraints, *SIAM/ASA J. Uncertainty Quantification* 2 (1) (2014) 364–396.
- [41] D. P. Kouri, M. Heinkenschloss, D. Ridzal, B. van Bloemen Waanders, Inexact objective function evaluations in a trust-region algorithm for PDE-constrained optimization under uncertainty, *SIAM Journal on Scientific Computing* 36 (6) (2014) A3011–A3029.
- [42] A. Kunoth, C. Schwab, Analytic regularity and GPC approximation for control problems constrained by linear parametric elliptic and parabolic PDEs, *SIAM Journal on Control and Optimization* 51 (3) (2013) 2442–2471.
- [43] L. Ng, K. Willcox, Multifidelity approaches for optimization under uncertainty, *International Journal for Numerical Methods in Engineering* 100 (10) (2014) 746–772. doi:10.1002/nme.4761.
- [44] P. Chen, A. Quarteroni, G. Rozza, Multilevel and weighted reduced basis method for stochastic optimal control problems constrained by Stokes equations, *Numerische Mathematik* 133 (1) (2016) 67–102.
- [45] A. Kunoth, C. Schwab, Sparse adaptive tensor Galerkin approximations of stochastic PDE-constrained control problems, *SIAM/ASA Journal on Uncertainty Quantification* 4 (1) (2016) 1034–1059.
- [46] D. P. Kouri, T. M. Surowiec, Risk-averse PDE-constrained optimization using the conditional value-at-risk, *SIAM Journal on Optimization* 26 (1) (2016) 365–396. doi:10.1137/140954556.
- [47] P. Benner, A. Onwunta, M. Stoll, Block-diagonal preconditioning for optimal control problems constrained by PDEs with uncertain inputs, *SIAM Journal on Matrix Analysis and Applications* 37 (2) (2016) 491–518.
- [48] A. A. Ali, E. Ullmann, M. Hinze, Multilevel Monte Carlo analysis for optimal control of elliptic PDEs with random coefficients, *SIAM/ASA Journal on Uncertainty Quantification* 5 (1) (2017) 466–492.
- [49] P. Chen, O. Ghattas, Taylor approximation for chance constrained optimization, preprint.
- [50] D. Colton, R. Kress, *Inverse acoustic and electromagnetic scattering theory*, Vol. 93, Springer Science & Business Media, 2012.
- [51] E. Turkel, A. Yefet, Absorbing pml boundary layers for wave-like equations, *Applied Numerical Mathematics* 27 (1998) 533–557.

- [52] B. Mueller, Additive manufacturing technologies—Rapid prototyping to direct digital manufacturing, *Assembly Automation* 32 (2).
- [53] R. Paul, S. Anand, F. Gerner, Effect of thermal deformation on part errors in metal powder based additive manufacturing processes, *Journal of Manufacturing Science and Engineering* 136 (3) (2014) 031009.
- [54] J. M. Pinto, C. Arrieta, M. E. Andia, S. Uribe, J. Ramos-Grez, A. Vargas, P. Irarrazaval, C. Tejos, Sensitivity analysis of geometric errors in additive manufacturing medical models, *Medical engineering & physics* 37 (3) (2015) 328–334.
- [55] F. Lindgren, H. Rue, J. Lindström, An explicit link between Gaussian fields and Gaussian Markov random fields: the stochastic partial differential equation approach, *Journal of the Royal Statistical Society: Series B (Statistical Methodology)* 73 (4) (2011) 423–498. doi:10.1111/j.1467-9868.2011.00777.x. URL <http://dx.doi.org/10.1111/j.1467-9868.2011.00777.x>
- [56] P. H. Flath, L. C. Wilcox, V. Akçelik, J. Hill, B. van Bloemen Waanders, O. Ghattas, Fast algorithms for Bayesian uncertainty quantification in large-scale linear inverse problems based on low-rank partial Hessian approximations, *SIAM Journal on Scientific Computing* 33 (1) (2011) 407–432. doi:10.1137/090780717.
- [57] T. Bui-Thanh, O. Ghattas, Analysis of the Hessian for inverse scattering problems. Part I: Inverse shape scattering of acoustic waves, *Inverse Problems* 28 (5) (2012) 055001. doi:10.1088/0266-5611/28/5/055001.
- [58] T. Bui-Thanh, O. Ghattas, Analysis of the Hessian for inverse scattering problems. Part III: Inverse medium scattering of electromagnetic waves, *Inverse Problems and Imaging* 7 (4) (2013) 1139–1155.
- [59] T. Bui-Thanh, O. Ghattas, Analysis of the Hessian for inverse scattering problems. Part II: Inverse medium scattering of acoustic waves, *Inverse Problems* 28 (5) (2012) 055002. doi:10.1088/0266-5611/28/5/055002.
- [60] T. Bui-Thanh, C. Burstedde, O. Ghattas, J. Martin, G. Stadler, L. C. Wilcox, Extreme-scale UQ for Bayesian inverse problems governed by PDEs, in: *SC12: Proceedings of the International Conference for High Performance Computing, Networking, Storage and Analysis*, 2012.
- [61] T. Bui-Thanh, O. Ghattas, J. Martin, G. Stadler, A computational framework for infinite-dimensional Bayesian inverse problems Part I: The linearized case, with application to global seismic inversion, *SIAM Journal on Scientific Computing* 35 (6) (2013) A2494–A2523. doi:10.1137/12089586X.
- [62] A. Alexanderian, N. Petra, G. Stadler, O. Ghattas, A fast and scalable method for A-optimal design of experiments for infinite-dimensional Bayesian nonlinear inverse problems, *SIAM Journal on Scientific Computing* 38 (1) (2016) A243–A272. doi:10.1137/140992564.
- [63] A. Alexanderian, N. Petra, G. Stadler, O. Ghattas, A-optimal design of experiments for infinite-dimensional Bayesian linear inverse problems with regularized ℓ_0 -sparsification, *SIAM Journal on Scientific Computing* 36 (5) (2014) A2122–A2148. doi:10.1137/130933381.
- [64] B. Crestel, A. Alexanderian, G. Stadler, O. Ghattas, A-optimal encoding weights for nonlinear inverse problems, with application to the Helmholtz inverse problem, *Inverse Problems* 33 (7) (2017) 074008. URL <http://iopscience.iop.org/10.1088/1361-6420/aa6d8e>
- [65] N. Petra, J. Martin, G. Stadler, O. Ghattas, A computational framework for infinite-dimensional Bayesian inverse problems: Part II. Stochastic Newton MCMC with application to ice sheet inverse problems, *SIAM Journal on Scientific Computing* 36 (4) (2014) A1525–A1555.
- [66] T. Isaac, N. Petra, G. Stadler, O. Ghattas, Scalable and efficient algorithms for the propagation of uncertainty from data through inference to prediction for large-scale problems, with application to flow of the Antarctic ice sheet, *Journal of Computational Physics* 296 (2015) 348–368. doi:10.1016/j.jcp.2015.04.047.
- [67] J. Martin, L. C. Wilcox, C. Burstedde, O. Ghattas, A stochastic Newton MCMC method for large-scale statistical inverse problems with application to seismic inversion, *SIAM Journal on Scientific Computing* 34 (3) (2012) A1460–A1487. doi:10.1137/110845598.
- [68] T. Bui-Thanh, O. Ghattas, A scalable MAP solver for Bayesian inverse problems with Besov priors, *Inverse Problems and Imaging* 9 (1) (2015) 27–54.
- [69] P. Chen, U. Villa, O. Ghattas, Hessian-based adaptive sparse quadrature for infinite-dimensional Bayesian inverse problems, *Computer Methods in Applied Mechanics and Engineering* 327 (2017) 147–172. URL <https://doi.org/10.1016/j.cma.2017.08.016>
- [70] P. Chen, O. Ghattas, Hessian-based sampling for high-dimensional model reduction, *International Journal for Uncertainty Quantification* 9 (2).
- [71] P. Chen, K. Wu, J. Chen, T. O’Leary-Roseberry, O. Ghattas, Projected Stein variational Newton: A fast and scalable Bayesian inference method in high dimensions, *Advances in Neural Information Processing Systems*.
- [72] P. Chen, O. Ghattas, Projected stein variational gradient descent, *arXiv preprint arXiv:2002.03469*.
- [73] N. Halko, P. G. Martinsson, J. A. Tropp, Finding structure with randomness: Probabilistic algorithms for constructing approximate matrix decompositions, *SIAM Review* 53 (2) (2011) 217–288.
- [74] A. K. Saibaba, J. Lee, P. K. Kitanidis, Randomized algorithms for generalized Hermitian eigenvalue problems with application to computing Karhunen–Loève expansion, *Numerical Linear Algebra with Applications* 23 (2) (2016) 314–339.

- [75] N. Alger, P. Chen, O. Ghattas, Tensor train construction from tensor actions, with application to compression of large high order derivative tensors, arXiv preprint arXiv:2002.06244, to appear in *SIAM Journal on Scientific Computing*.